J. Fluid Mech. (1985), *vol.* 158, *pp.* 289–316
Printed in Great Britain

On the stability of pipe-Poiseuille flow to finite-amplitude axisymmetric and non-axisymmetric disturbances

By P. K. SEN
Department of Applied Mechanics, Indian Institute of Technology, New Delhi 110016

D. VENKATESWARLU
Department of Mechanical Engineering, Delhi College of Engineering, Delhi 110006

AND S. MAJI
Department of Applied Mechanics, Indian Institute of Technology, New Delhi 110016

(Received 18 May 1983 and in revised form 2 January 1985)

The stability of fully developed pipe-Poiseuille flow to finite-amplitude axisymmetric and non-axisymmetric disturbances has been studied using the equilibrium-amplitude method of Reynolds & Potter (1967). In both the cases the least-stable centre-modes were investigated. Also, for the non-axisymmetric case the mode investigated was the one with azimuthal wavenumber equal to one. Many higher-order Landau coefficients were calculated, and the Stuart–Landau series was analysed by the Shanks (1955) method and by using Padé approximants to look for the existence of possible equilibrium states. The results show in both cases that, for each value of the Reynolds number R, there is a preferred band of spatial wavenumbers α in which equilibrium states are likely to exist. Moreover, in both cases it was found that the magnitude of the minimum threshold amplitude for a given R decreases with increasing R. The scales of the various quantities obtained agree very well with those deduced by Davey & Nguyen (1971).

1. Introduction

The study of the stability of fully-developed pipe-Poiseuille flow to finite-amplitude disturbances is important as this is likely to shed some light on the mechanism of breakdown of the orderly laminar flow. As regards infinitesimal disturbances, it is well known from past theoretical studies (e.g. Davey & Drazin 1969; Salwen & Grosch 1972; Garg & Rouleau 1972) that pipe-Poiseuille flow is stable to all modes of infinitesimal disturbances, whether axisymmetric or non-axisymmetric, for all points in the (α, R)-plane. There is also some experimental corroboration of these theoretical results, notably from the works of Leite (1959), Fox, Lessen & Bhat (1968) and Sarpkaya (1975). Consideration of these facts makes the study of finite-amplitude disturbances in pipe-Poiseuille flow all the more important.

It is now well known from the earlier theoretical work on the linear problem that, both for axisymmetric and non-axisymmetric disturbances, the least-stable mode is a centre-mode. Also, the least-stable centre-mode for non-axisymmetric disturbances, with azimuthal wavenumber equal to one, is even less stable than the least-stable axisymmetric centre-mode. It is therefore natural to believe that, if finite-amplitude

destabilization is to be expected, then this is most likely to occur for the cases of the least-stable centre-mode in both the axisymmetric and the non-axisymmetric cases. Thus, in the present work, the nonlinear problems corresponding to these two cases are investigated. The method of investigation used is the equilibrium-amplitude method of Reynolds & Potter (1967; hereinafter referred to as RP).

Some experiments have also been reported in the past on finite-amplitude effects in pipe-Poiseuille flow, especially in the earlier quoted references on experimental work. Unfortunately, all these results are for cases corresponding to wall modes. For example, the work of Fox *et al.* (1968) does consider finite-amplitude non-axisymmetric disturbances with azimuthal wavenumber one, but the disturbances correspond to phase speeds $c_r \approx 0.5$. Thus these experimental results do not shed any light on the behaviour of finite-amplitude disturbances for the least-stable centre-modes. It will be useful if such experimental results, with which the theoretical results could be compared, were to become available in future.

Regarding the theoretical works on nonlinear disturbances in pipe-Poiseuille flow, it seems that no earlier work, at least not any based on the Stuart (1960)–Watson (1960) formalism, exists for non-axisymmetric disturbances. As regards axisymmetric disturbances, there are two important earlier works. The first, due to Davey & Nguyen (1971), employs the RP method. In this work the first Landau coefficient was calculated for the least-stable centre-mode and for the least-stable wall-mode (which is more stable than the centre-mode). The sign of the Landau coefficient indicated possible destabilization of the flow due to finite-amplitude effects. In the second work, due to Itoh (1977*a*,*b*), again the first Landau coefficient was calculated based on an independent formulation developed by Itoh. However, the sign of the coefficient calculated by Itoh indicated further stabilization of the flow with finite-amplitude disturbances, for the least-stable centre-mode. Later, Davey (1978) attempted to explain this discrepancy. Davey also calculated the first Landau coefficient for the least-stable wall-mode, both by Itoh's theory and by the RP method. But these were found to be in qualitative agreement with each other, in contrast with the case of the least-stable centre-mode.

The motivation for the present work is therefore to make a detailed study of the problem of nonlinear stability of pipe-Poiseuille flow, so as to be able to arrive at a more convincing set of conclusions. A similar detailed work on plane-Poiseuille flow has been reported by Sen & Venkateswarlu (1983, hereinafter referred to as I).

2. Formulation

The formulation of the problem is considered with respect to the cylindrical polar form of the incompressible Navier–Stokes and continuity equations, with r, ϕ and x the radial, azimuthal and axial coordinates respectively, and with v, w and u the velocity components in the r-, ϕ- and x-directions respectively. All distances are normalized with respect to the pipe radius, and all velocities are normalized with respect to the centreline velocity of the undistorted laminar flow. The formulation is given separately for the axisymmetric and non-axisymmetric cases.

2.1. *Axisymmetric case*

In the axisymmetric case the problem is mathematically two-dimensional, and a stream function ψ can be introduced as follows:

$$u = \frac{1}{r}\frac{\partial \psi}{\partial r}, \quad v = -\frac{1}{r}\frac{\partial \psi}{\partial x}. \tag{1}$$

Further, after eliminating the pressure terms between the r- and x-components of the Navier–Stokes equations, one obtains the following equation in terms of ψ:

$$\left[\mathrm{N}-R\frac{\partial}{\partial t}\right]\mathrm{N}\psi = \frac{R}{r}\left[\frac{\partial\psi}{\partial r}\frac{\partial}{\partial x}-\frac{\partial\psi}{\partial x}\left(\frac{\partial}{\partial r}-\frac{2}{r}\right)\right]\mathrm{N}\psi, \tag{2}$$

where

$$\mathrm{N} \equiv \frac{\partial^2}{\partial r^2}-\frac{1}{r}\frac{\partial}{\partial r}+\frac{\partial^2}{\partial x^2},$$

and R is the Reynolds number.

In order to model the disturbances, ψ is assumed as composed of a mean part $\phi_0(r,t)$ and a perturbation consisting of a Fourier series of travelling waves, as follows:

$$\psi(x,r,t) = \phi_0(r,t)+\sum_{\substack{n=-\infty\\ n\neq 0}}^{\infty}\phi_n(r,t)\,\mathrm{e}^{\mathrm{i}n\alpha(x-c_r t)}, \tag{3}$$

where c_r is the phase speed according to linear theory and α is the x-wise spatial wavenumber. Also, for negative values of n, $\phi_{-n} = \tilde{\phi}_n$, where a tilde ($\tilde{}$) denotes the complex conjugate.

Further, as in I, the following expansions and conditions (*a*)–(*e*) are introduced.

(*a*) *Mean motion*:

$$\hat{U}(r,t) = U(r)+F(r,t), \quad U(r) = 1-r^2, \tag{4}$$

$$F(r,t) = \sum_{m=1}^{\infty}|A|^{2m} f_m^0(r). \tag{5}$$

where $U(r)$ is the undistorted laminar velocity, $\hat{U}(r,t)$ is the distorted mean velocity, and f_m^0 are the mean-motion distortion functions. Also, $A = A(t)$ is the (complex) amplitude ascribed to the fundamental disturbance.

(*b*) *The Stuart–Landau equation*:

$$\frac{\mathrm{d}A}{\mathrm{d}t} = \alpha c_i A+\mathrm{i}\alpha A\sum_{n=1}^{\infty}K_n|A|^{2n}, \tag{6}$$

$$S = \frac{1}{2\alpha|A|^2}\frac{\mathrm{d}|A|^2}{\mathrm{d}t} = c_i-\sum_{n=1}^{\infty}K_{ni}|A|^{2n}, \tag{7}$$

where K_n are the Landau coefficients, $c = c_r+\mathrm{i}c_i$ is the complex phase speed according to linear theory, and subscript i in K_{ni} denotes the imaginary part of K_n. Also, S represents the sum to infinity (correct sum) of the Stuart–Landau series in the form given in (7).

(*c*) *The harmonic distortion functions*:

$$\phi_n(r,t) = A^n\sum_{m=0}^{\infty}|A|^{2m}\psi_{nm}(r), \tag{8}$$

where ψ_{n0} will be referred to as ψ_n, and ψ_1 is the fundamental eigenfunction according to linear theory.

(*d*) *The equilibrium amplitude assumption of RP*:

$$\frac{\mathrm{d}|A|^2}{\mathrm{d}t} = 0. \tag{9}$$

If this assumption is not made, then the mean-motion equation will be subject to singularities (see Davey & Nguyen 1971).

(*e*) *It is assumed that the laminar pressure gradient* $\mathrm{d}p/\mathrm{d}x = -4/R$ *remains unaltered in the presence of disturbances.*

Substituting (3)–(9) in (2), and after some algebra, one obtains the differential equations corresponding to any f_m^0 and any ψ_{nm} respectively as follows:

$$f_m^{0\prime\prime}+\frac{1}{r}f_m^{0\prime} = \frac{\mathrm{i}\alpha R}{r^2}\sum_{n=1}^{m}\sum_{p=0}^{\substack{(p+d)\leqslant m\\ m-1}} n(\tilde{\psi}_{np}\,\mathrm{M}_n\,\psi_{n,\,m-p-n} - \psi_{np}\,\mathrm{M}_n\,\tilde{\psi}_{n,\,m-p-n}), \quad n=1,2,3,\ldots, \quad m=1,2,3,\ldots, \tag{10}$$

$$\begin{aligned}\mathrm{L}_n\psi_{nm} = {} & \mathrm{i}n\alpha R\sum_{p=1}^{m}\left[K_p\,\mathrm{M}_n\,\psi_{n,\,m-p}+f_p^0\,\mathrm{M}_n\,\psi_{n,\,m-p}-\left(f_p^{0\prime\prime}-\frac{1}{r}f_p^{0\prime}\right)\psi_{n,\,m-p}\right]\\ & +\frac{\mathrm{i}\alpha R}{r}\sum_{p=1}^{n-1}\sum_{d=0}^{m}[(n-p)\,\psi'_{pd}\,\mathrm{M}_{n-p}\,\psi_{n-p,\,m-d}-p\psi_{pd}\,\mathrm{M}^*_{n-p}\,\psi_{n-p,\,m-d}]\\ & +\frac{\mathrm{i}\alpha R}{r}\sum_{p=1}^{m}\sum_{d=0}^{m-1}[(n+p)\,\tilde{\psi}'_{pd}\,\mathrm{M}_{n+p}\,\psi_{n+p,\,m-p-d}\\ & +p\tilde{\psi}_{pd}\,\mathrm{M}^*_{n+p}\,\psi_{n+p,\,m-p-d}-p\psi'_{n+p,\,m-p-d}\,\mathrm{M}_p\,\tilde{\psi}_{pd}\\ & -(n+p)\,\psi_{n+p,\,m-p-d}-\mathrm{M}^*_p\,\tilde{\psi}_{pd}], \quad n=1,2,3,\ldots, \quad m=0,1,2,3,\ldots,\end{aligned} \tag{11}$$

where primes (′) denote differentiation with respect to r. The different operators in (10) and (11) are

$$\left.\begin{aligned}\mathrm{M}_n &\equiv \frac{\mathrm{d}^2}{\mathrm{d}r^2}-\frac{1}{r}\frac{\mathrm{d}}{\mathrm{d}r}-n^2\alpha^2,\\ \mathrm{M}^*_n &\equiv \left(\frac{\mathrm{d}}{\mathrm{d}r}-\frac{2}{r}\right)\mathrm{M}_n,\\ \overline{\mathrm{M}}_n &\equiv \mathrm{M}_n-n\mathrm{i}\alpha R\,(1-r^2-c),\\ \mathrm{L}_n &\equiv \overline{\mathrm{M}}_n\,\mathrm{M}_n.\end{aligned}\right\} \tag{12}$$

The boundary conditions for (10) and (11) are respectively

$$f_m^0 = 0 \quad \text{at } r=1, \quad f_m^{0\prime}=0 \quad \text{at } r=0, \tag{13}$$

$$\psi_{nm}=0, \quad \psi'_{nm}=0 \quad \text{at } r=0,1. \tag{14}$$

It is also known from Davey & Nguyen (1971) that f_m^0 and ψ_{nm} behave as even functions of r, near and at the centreline of the pipe.

Further, following Davey & Nguyen, the eigenfunction is normalized at the centreline such that $\psi_1''=2$ at $r=0$.

Again following Davey & Nguyen, the differential equation for the adjoint eigenfunction θ and the boundary conditions are

$$\overline{\mathrm{L}}_1\,\theta = \mathrm{M}_1\,\overline{\mathrm{M}}_1\,\theta = 0, \tag{15a}$$

$$\theta=\theta'=0 \quad \text{at } r=0,1. \tag{15b}$$

The equation for any ψ_{1n} function may be written in the following form from (11):

$$\mathrm{L}_1\,\psi_{1n} = \mathrm{i}\alpha R K_n\,\mathrm{M}_1\,\psi_1+T_{1n}. \tag{16}$$

Thus, by using the solvability condition for the equation for ψ_{1n}, i.e. (16), the Landau coefficient K_n may be determined as follows:

$$K_n = \frac{\int_0^1 \frac{1}{r}\theta T_{1n}\,\mathrm{d}r}{\mathrm{i}\alpha R\int_0^1 \frac{1}{r}\theta \mathrm{M}_1\psi_1\,\mathrm{d}r}. \tag{17}$$

Finally, it can also be seen from (16), that a normalization has to be specified for the ψ_{1n} functions. Similarly, for reasons described in I, the normalization adopted here is to exclude the ψ_1 content in the ψ_{1n} functions. This can be achieved by keeping $\psi''_{1n} = 0$ at $r = 0$, in addition to the boundary conditions given by (14).

2.2. *Non-axisymmetric case*

For the non-axisymmetric case, with the fundamental disturbance having azimuthal wavenumber one, the expressions for u, v, w and the pressure P are

$$\left.\begin{aligned} u = u^* + \hat{U}(r,t), \quad v = v^*, \quad w = w^*, \quad P = P^* + \bar{P}(x), \\ (u^*, v^*, w^*, P^*) = \sum_{\substack{n=-\infty \\ n\neq 0}}^{\infty} \left(F_n, \mathrm{i}\frac{n}{|n|}G_n, H_n, P_n\right)\mathrm{e}^{n(1\phi+1\alpha(x-c_r t))}, \end{aligned}\right\} \tag{18}$$

where an asterisk (*) indicates fluctuating parts. Also $\hat{U}(r,t)$ is the distorted mean velocity, $\bar{P}(x)$ is the (undistorted) mean pressure, c_r is the phase speed according to linear theory, α is the x-wise spatial wavenumber and n represents the order of the harmonic level. Further, $n = 1$ denotes the fundamental, and F_n, G_n, H_n and P_n represent complex amplitude functions for the nth harmonic level. Also, negative values of n indicate the complex conjugate, i.e. $F_{-n} = \tilde{F}_n$, where a tilde (~) denotes the complex conjugate.

Similarly to the axisymmetric case, the distorted mean velocity $\hat{U}(r,t)$, the undistorted laminar mean velocity $U(r)$ and the mean-motion distortion functions $F(r,t)$ are given by (4) and (5) for the present case.

Substituting (18) and (4) into the three components of the Navier–Stokes equations and the continuity equation and separating at various harmonic levels, one obtains the following set of equations respectively for the three components F_n, G_n and H_n, the mean-motion distortion F and the continuity equation:

$$n\alpha\left(\hat{U} - c_r - \frac{\mathrm{i}}{n\alpha}\frac{\partial}{\partial t}\right)F_n + \hat{U}'G_n + n\alpha P_n + \frac{\mathrm{i}}{R}\left[F''_n + \frac{1}{r}F'_n - n^2\left(\alpha^2 + \frac{1}{r^2}\right)F_n\right]$$
$$= -\sum_{\substack{p=-\infty \\ p\neq 0}}^{\infty}\left[(n-p)\alpha F_p F_{n-p} + \frac{p}{|p|}G_p F'_{n-p} + \frac{n-p}{r}H_p F_{n-p}\right], \tag{19}$$

$$n\alpha\left(\hat{U} - c_r - \frac{\mathrm{i}}{n\alpha}\frac{\partial}{\partial t}\right)G_n - P'_n + \frac{\mathrm{i}}{R}\left[G''_n + \frac{1}{r}G'_n - \left(n^2\alpha^2 + \frac{n^2+1}{r^2}\right)G_n - \frac{2n}{r^2}H_n\right]$$
$$= -\sum_{\substack{p=-\infty \\ p\neq 0}}^{\infty}\left[\frac{(n-p)^2}{|n-p|}\alpha F_p G_{n-p} + \frac{p}{|p|}\frac{n-p}{|n-p|}G_p G'_{n-p} + \frac{H_p}{r}\left\{\frac{(n-p)^2}{|n-p|}G_{n-p} + H_{n-p}\right\}\right], \tag{20}$$

$$n\alpha\left(\hat{U} - c_r - \frac{\mathrm{i}}{n\alpha}\frac{\partial}{\partial t}\right)H_n + \frac{nP_n}{r} + \frac{\mathrm{i}}{R}\left[H''_n + \frac{1}{r}H'_n - \left(n^2\alpha^2 + \frac{n^2+1}{r^2}\right)H_n - \frac{2n}{r^2}G_n\right]$$
$$= -\sum_{\substack{p=-\infty \\ p\neq 0}}^{\infty}\left[(n-p)\alpha F_p H_{n-p} + \frac{p}{|p|}G_p H'_{n-p} + \frac{H_p}{r}\left\{(n-p)H_{n-p} + \frac{n-p}{|n-p|}G_{n-p}\right\}\right], \tag{21}$$

$$F''+\frac{1}{r}F'-R\frac{\partial F}{\partial t}=\mathrm{i}R\sum_{\substack{p=-\infty\\ p\neq 0}}^{\infty}\left[-p\alpha F_p F_{-p}+\frac{p}{|p|}G_p F'_{-p}-\frac{p}{r}H_p F_{-p}\right], \tag{22}$$

$$n\alpha F_n+\frac{n}{|n|}G'_n+\frac{n}{|n|}\frac{G_n}{r}+n\frac{H_n}{r}=0. \tag{23}$$

We note at this stage that identical expressions and conditions (*a*)–(*e*), with the exception of (*c*), as given for the axisymmetric case in §2.1, are introduced here as well. In place of (*c*), the following expansions are introduced for the harmonic distortion functions:

$$[F_p(r,t),G_p(r,t),H_p(r,t)]=\sum_{q=0}^{\infty}[f_{pq}(r),g_{pq}(r),h_{pq}(r)]\,A^p\,|A|^{2q}, \tag{24}$$

with an analogous expression for the complex conjugate. Further, as before, expressions like f_{p0} (i.e. for $q=0$) corresponding to the principal component at the pth harmonic level, will be referred to as f_p.

The derivation, from (19) to (23) onwards, is proceeded with as follows. The fluctuating pressure terms P_n are eliminated between (19), (20) and (21) by cross-differentiation. The H_n function is eliminated on the left-hand sides (i.e. for the linear terms) by the use of the continuity equation in the form of (23). The equations and expansions given by (4)–(7), (9) and (24) are substituted. It may be noted also that if the equilibrium-amplitude assumption of RP (see (9)) is not made beforehand, then it can be seen from (22) that similarly to the axisymmetric case, in the present case also the mean-motion equation will be subject to singularities for $c_i<0$. Thus Watson's (1960) method would not be appropriate for either the axisymmetric or the non-axisymmetric problem.

After some heavy algebra, with the substitutions made as mentioned earlier, one obtains the continuity equation in terms of g_{nm}, f_{nm} and h_{nm}, the equation for the mean-motion distortion function f^0_m, and a pair of coupled equations, to be called the master equations, for g_{nm} and f_{nm}:

$$n\alpha f_{nm}+g'_{nm}+\frac{g_{nm}}{r}+\frac{nh_{nm}}{r}=0,\quad n=1,2,3,\ldots;\quad m=0,1,2,3,\ldots, \tag{25}$$

$$\begin{aligned}f^{0\prime\prime}_m+\frac{1}{r}f^{0\prime}_m=\mathrm{i}R\sum_{p=1}^{m}\sum_{\substack{d=0\\ (p+d)\leqslant m}}^{m-1}\Big[&-p\alpha(f_{pd}\tilde{f}_{p,\,m-p-d}-\tilde{f}_{pd}f_{p,\,m-p-d})\\&+g_{pd}\tilde{f}'_{p,\,m-p-d}-\tilde{g}_{pd}f'_{p,\,m-p-d}-\frac{p}{r}(h_{pd}\tilde{f}_{p,\,m-p-d}-\tilde{h}_{pd}f_{p,\,m-p-d})\Big],\\ &m=1,2,3,\ldots;\quad p=1,2,3,\ldots,\end{aligned} \tag{26}$$

$$\mathrm{L}_1(n\alpha)\,g_{nm}+\mathrm{L}_2(n\alpha)f_{nm}=N^{(1)}_{nm},\quad n=1,2,3,\ldots;\quad m=0,1,2,\ldots, \tag{27}$$

$$\mathrm{L}_3(n\alpha)\,g_{nm}+\mathrm{L}_4(n\alpha)f_{nm}=N^{(2)}_{nm},\quad n=1,2,3,\ldots;\quad m=0,1,2,\ldots, \tag{28}$$

where $N^{(1)}_{nm}$ and $N^{(2)}_{nm}$ are the nonlinear forcing terms.

Details of the left-hand sides of (27) and (28) are as follows (the expressions for $N^{(1)}_{nm}$ and $N^{(2)}_{nm}$ are very lengthy and are omitted here – interested readers may obtain copies of these on request, either from the authors or from the Editor):

$$
\begin{aligned}
&\mathrm{L}_1(n\alpha)\,g_{nm}+\mathrm{L}_2(n\alpha)f_{nm}\\
&\quad=g^{\mathrm{iv}}_{nm}+\frac{6}{r}g'''_{nm}-\left[\frac{n^2}{r^2}+\left\{n^2\alpha^2+\frac{n^2-5}{r^2}+\mathrm{i}n\alpha R(U-c)\right\}\right]g''_{nm}\\
&\qquad-\left[\frac{1}{r}\left\{\frac{2n^2+1}{r^2}+3n^2\alpha^2+3\mathrm{i}n\alpha R(U-c)+\mathrm{i}n\alpha RrU'\right\}\right]g'_{nm}\\
&\qquad+\left[\frac{1}{r^2}\left\{n^2\alpha^2+\frac{n^2-1}{r^2}+\mathrm{i}n\alpha R(U-c)\right\}(n^2-1)-\frac{\mathrm{i}n\alpha RU'}{r}\right]g_{nm}\\
&\qquad+n\alpha f'''_{nm}+\frac{5n\alpha}{r}f''_{nm}-n\alpha\left[n^2\alpha^2+\frac{n^2-3}{r^2}+\mathrm{i}n\alpha R(U-c)\right]f'_{nm}\\
&\qquad-\frac{n^2\alpha}{r}\left[2n\left(\alpha^2+\frac{1}{r^2}\right)+\mathrm{i}\alpha R\{2(U-c)+U'r\}\right]f_{nm}\\
&\quad=N^{(1)}_{nm},
\end{aligned}
\tag{27'}
$$

$$
\begin{aligned}
&\mathrm{L}_3(n\alpha)\,g_{nm}+\mathrm{L}_4(n\alpha)f_{nm}\\
&\quad=\alpha r^2 g'''_{nm}+4\alpha r g''_{nm}-\alpha r^2\left[n^2\alpha^2+\frac{n^2-1}{r^2}+\mathrm{i}n\alpha R(U-c)\right]g'_{nm}\\
&\qquad-\left[\alpha r\left\{n^2\alpha^2-\frac{n^2-1}{r^2}+\mathrm{i}n\alpha R(U-c)\right\}+\mathrm{i}nRU'\right]g_{nm}\\
&\qquad+n(1+\alpha^2r^2)f''_{nm}+\frac{n}{r}(1+3\alpha^2r^2)f'_{nm}\\
&\qquad-n(1+\alpha^2r^2)\left[n^2\left(\alpha^2+\frac{1}{r^2}\right)+\mathrm{i}n\alpha R(U-c)\right]f_{nm}\\
&\quad=N^{(2)}_{nm}.
\end{aligned}
\tag{28'}
$$

An important case obtainable from the master equations (27) and (28) is the case corresponding to the fundamental disturbance, which has $n = 1$ and $m = 0$, and for which case the right-hand-side terms $N^{(1)}_1$ and $N^{(2)}_1$ are identically zero. Thus one obtains the equations for the fundamental disturbance mode, corresponding to the linear eigenvalue problem, in the following form:

$$\mathrm{L}_1(\alpha)\,g_1+\mathrm{L}_2(\alpha)f_1=0, \tag{29}$$

$$\mathrm{L}_3(\alpha)\,g_1+\mathrm{L}_4(\alpha)f_1=0. \tag{30}$$

The solution procedure, for given n and m, is to solve for g_{nm} and f_{nm} from (27) and (28) and thereafter to obtain h_{nm} from the continuity equation (25). Also, f^0_m is obtained by solving (26). As regards the K_n coefficients, the solution procedure will be described subsequently.

Next we consider the boundary conditions. The boundary conditions for a similar problem (on axisymmetric jets) were first proposed by Batchelor & Gill (1962), and the boundary conditions for the linear problems of disturbances in pipe flow were given by Salwen & Grosch (1972) and Garg & Rouleau (1972). At the wall, $r = 1$, the boundary conditions are given by the no-slip condition. This gives

$$g_{nm}=0,\quad f_{nm}=0,\quad h_{nm}=0,\quad f^0_m=0\quad\text{at } r=1. \tag{31}$$

Further, from the continuity equation (25) it is seen that the following condition is also valid for g_{nm}:

$$g'_{nm}=0\quad\text{at } r=1. \tag{32}$$

At the centreline of the pipe, $r = 0$, the boundary conditions may formally be given for g_{nm}, depending on whether g_{nm} is odd or even with respect to r. Here the term 'odd' implies that the function itself and its even-order derivatives are zero for $r\to 0$,

and the term 'even' implies that the odd-order derivatives of the function are zero for $r \to 0$. It is known from past work (cf. Salwen & Grosch 1972; Garg & Rouleau 1972) that the eigensolution for the fundamental, corresponding to the least-stable mode, has g_1 as an even function with respect to r, with g_1 non-zero at $r = 0$. Thus the set of functions subsequently obtained has the following character, as may be deduced from (25), (27) and (28). First, for given n and m, if g_{nm} is even with respect to r then h_{nm} is also even and f_{nm} is odd. Also, if g_{nm} is odd then h_{nm} is odd and f_{nm} is even. Secondly, for odd values of the integer n, the g_{nm} functions are even, and, for even values of n, g_{nm} are odd. Further, it may also be deduced from (26) that f_m^0 is even for all integer values of m. The formal boundary conditions at $r = 0$, for (26)–(28), are therefore

$$\left.\begin{aligned} & f_m^{0\prime} = 0 \quad \text{at } r = 0, \\ & g'_{nm} = g'''_{nm} = 0, \quad f_{nm} = f''_{nm} = 0 \quad \text{at } r = 0, \quad \text{for } n = 1, 3, 5, \ldots, \\ & g_{nm} = g''_{nm} = 0; \quad f'_{nm} = f'''_{nm} = 0 \quad \text{at } r = 0, \quad \text{for } n = 2, 4, 6, \ldots. \end{aligned}\right\} \tag{33}$$

As far as the numerical solution is concerned, it seems that some additional information is necessary in view of the fact that the differential equations (25)–(28) portray singularities at $r = 0$. Thus the specific forms of g_{nm}, f_{nm}, h_{nm} and f_m^0 need to be known for $r \to 0$, in order to avoid singularities in the numerical work. With reference to (19)–(21), it is seen that generally speaking the g_{nm}, f_{nm} and h_{nm} functions should behave as r^p, with $p \geqslant 2$ for $r \to 0$, if singularities at $r = 0$ are to be avoided. There are, however, important exceptions to this rule, which may be deduced from (25), (27) and (28). The forms corresponding to even g_{nm} are thus

$$\left.\begin{aligned} g_{nm} &= g_{nm}^{(0)} + g_{nm}^{(0)\prime\prime} \frac{r^2}{2!} + g_{nm}^{(0)\mathrm{iv}} \frac{r^4}{4!} + \ldots, \\ h_{nm} &= h_{nm}^{(0)} + h_{nm}^{(0)\prime\prime} \frac{r^2}{2!} + h_{nm}^{(0)\mathrm{iv}} \frac{r^4}{4!} + \ldots, \\ f_{nm} &= f_{nm}^{(0)\prime} r + f_{nm}^{(0)'''} \frac{r^3}{3!} + \ldots, \quad n = 1, 3, 5, \ldots; \quad m = 0, 1, 2, 3, \ldots, \end{aligned}\right\} \tag{34}$$

where superscript (0) refers to values at $r = 0$. In (34) the following additional features are also valid. First, for $n \geqslant 3$, $g_{nm}^{(0)} = 0$, $h_{nm}^{(0)} = 0$ and $f_{nm}^{(0)\prime} = 0$. Secondly, it may be seen from (25) that, for the specific cases of $n = 1$ and $n = 3$, the following conditions are also respectively valid:

$$\left.\begin{aligned} g_{1m}^{(0)} + h_{1m}^{(0)} &= 0, \\ g_{3m}^{(0)\prime\prime} + h_{3m}^{(0)\prime\prime} &= 0. \end{aligned}\right\} \quad m = 0, 1, 2, 3, \ldots. \tag{35a, 35b}$$

The forms corresponding to odd g_{nm} are

$$\left.\begin{aligned} g_{nm} &= g_{nm}^{(0)\prime} r + g_{nm}^{(0)'''} \frac{r^3}{3!} + \ldots, \\ h_{nm} &= h_{nm}^{(0)\prime} r + h_{nm}^{(0)'''} \frac{r^3}{3!} + \ldots, \\ f_{nm} &= f_{nm}^{(0)\prime\prime} \frac{r^2}{2!} + f_{nm}^{(0)\mathrm{iv}} \frac{r^4}{4!} + \ldots, \\ & n = 2, 4, 6, \ldots; \quad m = 0, 1, 2, 3, \ldots. \end{aligned}\right\} \tag{36}$$

In (36) the following additional features are also valid. First, for $n \geqslant 4$, $g_{nm}^{(0)'} = 0$ and $h_{nm}^{(0)'} = 0$. Secondly, $f_{nm}^{(0)} = 0$ for all n. Thirdly, it may be seen from (25) that, for the specific case of $n = 2$, the following condition is also valid:

$$g_{2m}^{(0)'} + h_{2m}^{(0)'} = 0, \quad m = 0, 1, 2, 3, \ldots. \tag{37}$$

Further, it may be deduced from the right-hand side of (26) that the mean-motion distortion functions f_m^0 are even for all values of m. Thus the form for f_m^0 at $r \to 0$ is the same as that for g_{nm} with $n = 1$ in (34).

Thus (34)–(37) give further insight into the nature of the various functions for $r \to 0$. This helps not only in avoiding singularities in the numerical work but also in preadjusting the numerical work for better accuracy in the results. A specific set of examples, from the viewpoint of facility in numerical work, is discussed next. In the numerical work it is necessary to consider the differential equations (26)–(28) in their limiting forms at $r = 0$. In (26) this was found necessary for all orders in m, whereas, in (27) and (28) this was found necessary for the specific cases of $n = 1$ with $m = 0, 1, 2, 3, \ldots$. For $n > 1$ it was not necessary to consider the point at $r = 0$ in (27) and (28) in the numerical work, since the functions g_{nm} and f_{nm} are known to be zero at $r = 0$ (see (34) and (36)). The limiting form for (26) at $r = 0$ is

$$2f_m^{0''} = Q \quad \text{at } r = 0, \quad m = 1, 2, 3, \ldots, \tag{38}$$

where Q represents the limit of the right-hand-side terms in (26) at $r = 0$. Similarly the limiting forms of (27) and (28) at $r = 0$, for the specific case of $n = 1$ and $m = 0$ (i.e. for (29) and (30)), are respectively

$$8g_1^{\mathrm{iv}} - 4[\alpha^2 + \mathrm{i}\alpha R(1-c)]\,g_1'' + 2\mathrm{i}\alpha R g_1 + \tfrac{20}{3}\alpha f_1''' - 3\alpha[\alpha^2 + \mathrm{i}\alpha R(1-c)]\,f_1' = 0 \quad \text{at } r = 0, \tag{39}$$

$$4\alpha g_1'' - [\alpha^3 + \mathrm{i}\alpha^2 R(1-c) - 2\mathrm{i}R]\,g_1 + \tfrac{4}{3}f_1''' + [\alpha^2 - \mathrm{i}\alpha R(1-c)]\,f_1' = 0 \quad \text{at } r = 0. \tag{40}$$

The matter of considering the limits at $r = 0$ has to be taken into account in the right-hand sides of (26)–(28) as well. Fortunately, since the right-hand sides are known functions, having been calculated at earlier stages, the limits may be worked out either analytically or may be generated in the computer itself by a finite-difference technique. Computations up to K_3 were made using both these procedures for cross-checking the numerical work. For higher orders in K_n the limits were generated in the computer.

Next, the formal solutions for the K_n coefficients have to be developed. This requires defining an adjoint system to the system of equations for the fundamental, i.e. (29) and (30). The adjoint functions are called ϕ and ψ, and the adjoint equations are

$$\mathrm{L}_1^*(\alpha)\,\phi + \mathrm{L}_2^*(\alpha)\,\psi = 0, \tag{41}$$

$$\mathrm{L}_3^*(\alpha)\,\phi + \mathrm{L}_4^*(\alpha)\,\psi = 0, \tag{42}$$

where $\mathrm{L}_1^*(\alpha)$, $\mathrm{L}_2^*(\alpha)$, $\mathrm{L}_3^*(\alpha)$ and $\mathrm{L}_4^*(\alpha)$ are respectively the operators adjoint to $\mathrm{L}_1(\alpha)$, $\mathrm{L}_3(\alpha)$, $\mathrm{L}_2(\alpha)$ and $\mathrm{L}_4(\alpha)$ as given in (29) and (30). The expanded forms of (41) and (42) are

$$\phi^{\mathrm{iv}} - \frac{6}{r}\phi''' + \left[\frac{21}{r^2} - \{\alpha^2 + \mathrm{i}\alpha R(U-c)\}\right]\phi'' + \left[-\frac{45}{r^3} + \frac{3}{r}\{\alpha^2 + \mathrm{i}\alpha R(U-c)\} + 2\mathrm{i}\alpha R r\right]\phi'$$

$$+ \left[\frac{45}{r^4} - \frac{3}{r^2}\{\alpha^2 + \mathrm{i}\alpha R(U-c)\} - 4\mathrm{i}\alpha R\right]\phi - \alpha r^2\psi''' - 2\alpha R\psi'' + \alpha[r^2\{\alpha^2 + \mathrm{i}\alpha R(U-c)\} + 2]\,\psi'$$

$$+ [\alpha R\{\alpha^2 + \mathrm{i}\alpha R(U-c)\} - 2\mathrm{i}R\alpha^2 r^3 + 2\mathrm{i}rR]\,\psi = 0, \tag{41'}$$

$$-\alpha\phi'''+\frac{5\alpha}{r}\phi''-\alpha\left[\frac{12}{r^2}-\{\alpha^2+\mathrm{i}\alpha R(U-c)\}\right]\phi'+\alpha\left[\frac{12}{r^3}-\frac{2}{r}\{\alpha^2+\mathrm{i}\alpha R(U-c)\}\right]\phi$$

$$+(\alpha^2 r^2+1)\psi''+\left(\alpha^2 r-\frac{1}{r}\right)\psi'-\left[\alpha^2 r^2\left(\alpha^2+\frac{3}{r^2}\right)+\mathrm{i}\alpha R(U-c)(1+\alpha^2 r^2)\right]\psi=0. \quad (42')$$

The boundary conditions for the adjoint system are determined at the wall, $r = 1$, by considering the vanishing of the bilinear concomitant. This gives the following conditions at the wall:

$$\phi=\phi'=0, \quad \psi=0 \quad \text{at } r=1. \quad (43)$$

At the centreline, $r = 0$, again the boundary conditions for ϕ and ψ are given by the vanishing of singularities at $r = 0$. It is seen from (41′) and (42′) that ϕ is an odd function and ψ is an even function with respect to r, for $r \to 0$. Thus the boundary conditions at $r = 0$ are

$$\phi=\phi'=0, \quad \psi'=\psi'''=0 \quad \text{at } r=0. \quad (44)$$

Further, the limiting form for ϕ and ψ for $r \to 0$ may be deduced from (41′) and (42′):

$$\left.\begin{aligned}\phi &= \phi^{(0)\prime} r+\phi^{(0)'''}\frac{r^3}{3!}+\ldots,\\ \psi &= \psi^{(0)''}\frac{r^2}{2!}+\psi^{(0)\mathrm{iv}}\frac{r^4}{4!}+\ldots.\end{aligned}\right\} \quad (45)$$

Note in (45) that $\psi^{(0)} = 0$, although ψ is even with respect to r.

The system of equations for the fundamental as well as for the adjoint constitute eigenvalue problems for the same set of eigenvalues α, R and c. It is seen from (29) and (30), and also from (41) and (42), that a normalization has to be specified for the respective solutions for each of these two sets of equations. For the respective systems the normalizations adopted were $g_1 = 1$ at $r = 0$ and $\phi' = 1$ at $r = 0$.

To proceed with the determination of K_m, it is seen from (27′) and (28′) that the equations for any pair of g_{1m} and f_{1m} for $m \geqslant 1$ are

$$\mathrm{L}_1(\alpha)\, g_{1m}+\mathrm{L}_2(\alpha) f_{1m}=N_{1m}^{(1)}=K_m P_1-Q_1, \quad (46)$$

$$\mathrm{L}_3(\alpha)\, g_{1m}+\mathrm{L}_4(\alpha) f_{1m}=N_{1m}^{(2)}=K_m P_2-Q_2, \quad (47)$$

where $N_{1m}^{(1)}$ and $N_{1m}^{(2)}$ have each been split into two parts; one containing K_m and the other not containing K_m. The Landau coefficients K_m may be determined from the orthogonality condition of the right-hand side of the system of equations (46) and (47), and this is actually the solvability condition. Upon taking the inner product of (ϕ, ψ) with the right-hand-side term $(K_m P_1-Q_1, K_m P_2-Q_2)$, one obtains the following conditions:

$$\int_0^1 \phi(K_m P_1-Q_1)\,\mathrm{d}r+\int_0^1 \psi(K_m P_2-Q_2)\,\mathrm{d}r=0 \quad (48)$$

or

$$K_m=\frac{\int_0^1 (\phi Q_1+\psi Q_2)\,\mathrm{d}r}{\int_0^1 (\phi P_1+\psi P_2)\,\mathrm{d}r}. \quad (49)$$

Thus the Landau coefficient K_m may be determined from (49) at the stage of solution of the g_{1m} function. Again, it is seen from (46) and (47) that a normalization has to be specified for the solution of this set of equations as well. Similarly to I to §2.1 here for the axisymmetric case, the normalization adopted was to exclude the g_1 content in the g_{1m} functions; and incidentally this automatically excludes the f_1 content in the f_{1m} functions and the h_1 content in the h_{1m} functions. It can be shown, as in I, that this is achieved by specifying $g_{1m} = 0$ at $r = 0$.

3. Numerical methods

The numerical method used for solving the various differential equations is very similar to that described in I, that is by using an extended form of Thomas's (1953) method. However, owing to the presence of third derivative terms in the various differential equations of the present problem, a seven-point finite-difference scheme had to be used. Also, the following auxiliary function g was found to improve the accuracy considerably:

$$g = \phi - \tfrac{7}{20}h^2\phi'' + \tfrac{77}{1200}h^4\phi^{\mathrm{iv}} - \tfrac{63}{8000}h^6\phi^{\mathrm{vi}}, \tag{50a}$$

$$\phi = g + \tfrac{7}{20}\delta^2 g + \tfrac{7}{240}\delta^4 g + 0(h^8), \tag{50b}$$

where ϕ represents the actual function, δ is the central-difference operator and h is the step size. With the use of g as in (50a,b) the error in the derivatives is kept to $O(h^6)$. Nevertheless, Thomas's original auxiliary function can also be used in conjunction with a seven-point scheme with errors $O(h^4)$. The accuracy of computations was checked by using (50a,b) as well as by using Thomas's original auxiliary function.

The numerical work for the axisymmetric case was cross-checked with Davey & Nguyen's (1971) results for the first Landau coefficient. The details are given in table 3. Also, the results for K_n were obtained by the adjoint method (see (17)) and cross-checked by the matrix method described in I. The right-hand-side terms in (10) and (11) were generated in the computer as described in I, and the calculations up to K_3 were cross-checked by working out the right-hand-side expressions by hand and then feeding these expressions into the computer.

For the non-axisymmetric case, auxiliary functions λ and μ were defined respectively for g_{nm} and f_{nm}. Upon discretizing (27) and (28) by finite differences, the following system of algebraic equations are obtained:

$$[A_{ij}^{(1)}][\lambda_j] + [A_{ij}^{(2)}][\mu_j] = [P_i^{(1)}], \quad i,j = 1,2,3,\ldots,N+1, \tag{51}$$

$$[A_{ij}^{(3)}][\lambda_j] + [A_{ij}^{(4)}][\mu_j] = [P_i^{(2)}], \quad i,j = 1,2,3,\ldots,N+1, \tag{52}$$

where $[A_{ij}^{(p)}]$ are the respective matrix equivalents of the operators $\mathrm{L}_p(n\alpha)$, $p = 1,2,3,4$, $[P_i^{(1)}]$ and $[P_i^{(2)}]$ are respectively the discretized right-hand-side forcing terms $N_{nm}^{(1)}$ and $N_{nm}^{(2)}$, and N is the number of steps used in the finite-difference procedure. Also, i, j represent the station positions along r. Each of the $[A_{ij}^{(p)}]$ is a heptadiagonal band matrix of size $(N+1)\times(N+1)$. If (51) and (52) are to be solved simultaneously, then a rearrangement of these equations helps. It is easy to see that, for any ith location, if λ_j terms and μ_j terms are written alternately, then (51) and (52) reduce to a single matrix equation in the form

$$[A_{IJ}][\Gamma_J] = [P_I], \quad I,J = 1,2,3,\ldots,2N+2, \tag{53}$$

where $[A_{IJ}]$ is a fifteen-diagonal band matrix of size $(2N+2)\times(2N+2)$ consisting of all the four $[A_{ij}^{(p)}]$ but with the elements rearranged. Also, $[\Gamma_J]$ is the combined $[\lambda_j]$,

$[\mu_j]$ vector, with λ_j and μ_j appearing as alternate elements. Similarly $[P_I]$ is the combined $[P_i^{(1)}]$, $[P_i^{(2)}]$ vector with $P_i^{(1)}$ and $P_i^{(2)}$ appearing as alternate elements. Further, the correspondence between I, J and i, j is as follows. Any given i (or j) corresponds to a physical station in r, defined as $r = (i-1)h$, where h is the step size. For a given i, I will have two values, viz $I = 2i-1$ and $I = 2i$. Finally, we mention, that with the matrix equations given as in (53) with $[A_{IJ}]$ in banded form, the storage space is very considerably reduced, and the Gaussian-elimination procedure is very much simplified.

The solution of the matrix equation (53) is similar to that described in I. We only mention here that, as in I the K_n coefficients for the present problem were also determined by two methods, viz by the adjoint method (see (49)) and by the matrix method. Also, the right-hand-side terms in (26) and the terms $N_{nm}^{(1)}$ and $N_{nm}^{(2)}$ in (27) and (28) were generated in the computer as in I. Again, as in I, calculations up to K_3 were checked out by working out the algebra of $N_{nm}^{(1)}$ and $N_{nm}^{(2)}$ by hand and then feeding these expressions into the computer.

It may be seen from (27) and (28) that the volume of algebra involved in the non-axisymmetric case is considerably greater than in I or than in the axisymmetric case. For instance at the K_3 level itself, the full expression for $N_{13}^{(1)}$ contains over 170 terms.

The calculations were performed in an ICL 2960 computer in the Indian Institute of Technology, Delhi, using double-precision arithmetic.

4. Results and discussions

4.1. *Broad nature of the K_{ni} coefficients*

The analysis of the results begins with the inspection of the K_{ni} coefficients obtained. Typical values of the K_{ni} coefficients are given for the axisymmetric and non-axisymmetric cases respectively in tables 1 and 2. Domb–Sykes plots for the two cases are given respectively in figures 1 and 2. At first glance the plots appear rather irregular. However, the plot for the axisymmetric case depicts a periodicity of four and that for the non-axisymmetric case a periodicity of two. Plots of $|K_{ni}/K_{(n-4)i}|^{\frac{1}{4}}$ and $|K_{ni}/K_{(n-2)i}|^{\frac{1}{2}}$, also shown respectively in figures 1 and 2, confirm these. Figures 1 and 2 both seem to show that the nearest singularity in both cases is a simple pole. The periodicity of four in the plot for the axisymmetric case is suggestive of a complex-conjugate secondary singularity close to the circle of convergence. For the non-axisymmetric case the periodicity of two is suggestive of a secondary singularity in the form of a simple pole close to the circle of convergence either on the negative real axis or close to the primary singularity. The proximity of secondary singularities to the circle of convergence, in both cases, creates situations that would make a ready estimation of equilibrium amplitude (i.e. the zero-crossing of the series (7)) rather difficult, especially if the zero-crossing occurs close to the nearest singularity. It is believed that one possible reason for the irregularity of the K_{ni} coefficients is that the forced solutions for the harmonics are rather ill-conditioned, since the values of $n\alpha$ and c used at the nth-harmonic level are close to the eigenvalues for the free solution at that level.

Further examination of the K_{ni} coefficients, for different values of α at a given R, shows that both in the axisymmetric as well as in the non-axisymmetric cases there is a narrow band of α, which we will term the 'preferred band of α', where all the K_{ni} coefficients are of the same negative sign. This preferred band scales with $\alpha R^{-\frac{1}{3}}$,

	$\alpha = 11.0$, $R = 6000$, $\alpha R^{-\frac{1}{3}} = 0.6054$, $c_r = 0.98899$, $c_i = -0.012843$, $A_e = 0.0023062$			$\alpha = 9.0$, $R = 4000$, $\alpha R^{-\frac{1}{3}} = 0.5670$, $c_r = 0.98509$, $c_i = -0.017157$, $A_e = 0.0031677$	$\alpha = 9.6$, $R = 4000$, $\alpha R^{-\frac{1}{3}} = 0.6048$, $c_r = 0.98557$, $c_i = -0.016834$, $A_e = 0.0030168$	$\alpha = 10.2$, $R = 4000$, $\alpha R^{-\frac{1}{3}} = 0.6426$, $c_r = 0.98600$, $c_i = -0.016553$, $A_e = 0.0032228$
n	K_{nr}	K_{ni}	A_n ($\times 10^{-2}$)	K_{ni}	K_{ni}	K_{ni}
1	1.6898×10	-1.1691×10^{2}	1.04810	-8.5578×10	-8.9171×10	-9.1878×10
2	-5.9111×10^{6}	-1.6087×10^{7}	0.49854	-6.4274×10^{6}	-7.1617×10^{6}	-7.8596×10^{6}
3	-9.8991×10^{11}	-7.1495×10^{11}	0.43521	-9.9923×10^{10}	-1.8714×10^{11}	-2.9560×10^{11}
4	5.1730×10^{16}	-4.6966×10^{16}	0.40526	4.9825×10^{15}	-6.9965×10^{15}	-2.2618×10^{16}
5	1.5143×10^{22}	-3.1888×10^{22}	0.34296	-1.3023×10^{21}	-2.7788×10^{21}	-4.4275×10^{21}
6	-7.8009×10^{26}	-6.1834×10^{27}	0.31494	-1.8442×10^{26}	-3.1780×10^{26}	-4.3864×10^{26}
7	-1.6133×10^{31}	-4.0891×10^{32}	0.30685	-7.4940×10^{29}	-1.2524×10^{31}	-2.3147×10^{31}
8	1.0661×10^{38}	-5.9778×10^{37}	0.29991	4.5005×10^{35}	-1.0327×10^{36}	-2.4912×10^{36}
9	1.4896×10^{43}	-2.9354×10^{43}	0.28631	-1.0933×10^{41}	-2.9539×10^{41}	-4.3405×10^{41}
10	1.9213×10^{47}	-5.3096×10^{48}	0.27789	-1.2683×10^{46}	-3.1724×10^{46}	-3.6989×10^{46}
11	4.0453×10^{53}	-4.8350×10^{53}	0.27439	3.6352×10^{50}	-1.7183×10^{51}	-1.4270×10^{51}
12	1.7162×10^{59}	-1.1838×10^{59}	0.27012	2.0658×10^{55}	-2.2737×10^{56}	-1.1147×10^{56}
13	2.1634×10^{64}	-3.6613×10^{64}	0.26470	-1.5972×10^{61}	-4.3007×10^{61}	-9.6886×10^{60}
14	2.0453×10^{69}	-5.1772×10^{69}	0.26151	-1.0615×10^{66}	-3.6478×10^{66}	2.4417×10^{66}

TABLE 1. Typical results for the axisymmetric case. The equilibrium amplitude A_e is based on (7×7) Padé approximants. A_n is the equilibrium amplitude based on direct sum of series up to the K_{ni}th term.

	$\alpha = 3.0,\ R = 5000,\ \alpha R^{-\frac{1}{3}} = 0.1754,$ $c_r = 0.96069,\ c_i = -0.017879,\ A_e = 0.0015350$			$\alpha = 2.0,$ $R = 4000,$ $\alpha R^{-\frac{1}{3}} = 0.1260,$ $c_r = 0.94594,$ $c_i = -0.024929,$ A_e is unreliable	$\alpha = 3.0,$ $R = 4000,$ $\alpha R^{-\frac{1}{3}} = 0.1890,$ $c_r = 0.95612,$ $c_i = -0.019869,$ $A_e = 0.0018924$	$\alpha = 4.25,$ $R = 4000,$ $\alpha R^{-\frac{1}{3}} = 0.2677,$ $c_r = 0.96370,$ $c_i = -0.015995,$ A_e is unreliable
n	K_{nr}	K_{ni}	A_n $(\times 10^{-2})$	K_{ni}	K_{ni}	K_{ni}
1	-7.2067×10^{2}	-8.7878×10	1.42640	-3.8516×10	-8.1590×10	-9.1105×10
2	-5.7791×10^{7}	-1.7262×10^{7}	0.54533	-9.7745×10^{6}	-1.0746×10^{7}	-6.4312×10^{6}
3	-7.8756×10^{12}	-9.3504×10^{12}	0.34039	-3.5915×10^{12}	-4.1992×10^{12}	-1.8049×10^{12}
4	-2.2143×10^{18}	-2.5152×10^{18}	0.28516	1.8413×10^{17}	-8.3116×10^{17}	-1.7400×10^{17}
5	-6.2228×10^{23}	-1.0589×10^{24}	0.25072	1.9524×10^{23}	-2.4161×10^{23}	-2.2269×10^{22}
6	-1.7322×10^{29}	-4.3545×10^{29}	0.22956	1.0127×10^{29}	-6.6704×10^{28}	-8.5287×10^{26}
7	-3.9933×10^{34}	-1.8586×10^{35}	0.21517	4.0994×10^{34}	-1.8838×10^{34}	2.5412×10^{32}
8	-4.9083×10^{39}	-7.8529×10^{40}	0.20500	1.6229×10^{40}	-5.2064×10^{39}	1.0610×10^{38}

TABLE 2. Typical results for the non-axisymmetric case. The equilibrium amplitude A_e is based on (4×4) Padé approximants. A_n is the equilibrium amplitude based on direct sum of series up to the K_{ni}th term.

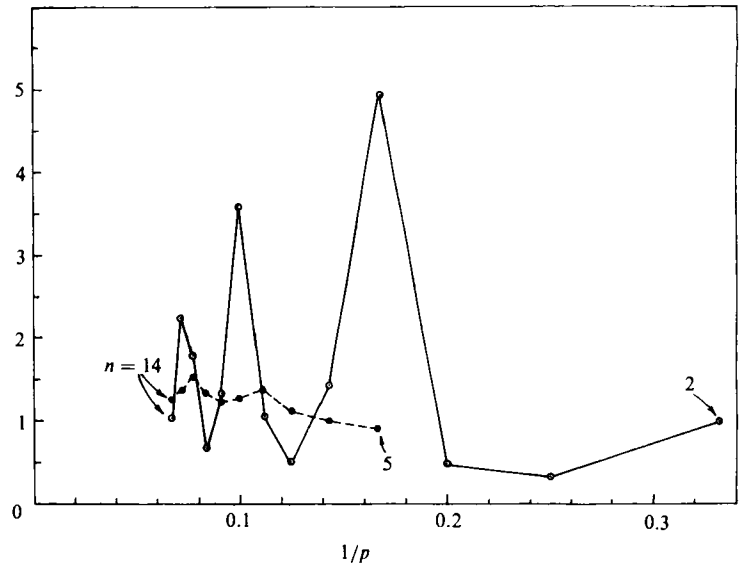

FIGURE 1. Domb–Sykes plots for $\alpha = 11.0$, $R = 6000$, axisymmetric case. Solid line is for $\frac{|K_{n1}/K_{(n-1)1}|}{|K_{21}/K_{11}|}$ and broken line is for $\frac{|K_{n1}/K_{(n-4)1}|^{\frac{1}{4}}}{|K_{21}/K_{11}|}$. Also $p = n+1$, where n is of the order of K_{n1}. Best estimate of r_c from above plots is $r_c = 0.0023$. By (7×7) Padé approximants, $r_c = 0.002314$.

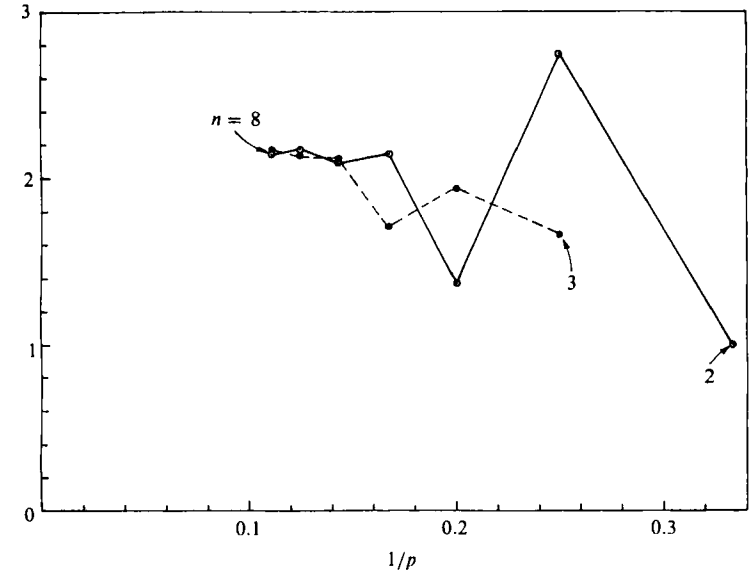

FIGURE 2. Domb–Sykes plots for $\alpha = 3.0$, $R = 5000$, non-axisymmetric case. Solid line is for $\frac{|K_{n1}/K_{(n-1)1}|}{|K_{21}/K_{11}|}$ and broken line is for $\frac{|K_{n1}/K_{(n-2)1}|^{\frac{1}{2}}}{|K_{21}/K_{11}|}$. Also $p = n+1$, where n is of the order of K_{n1}. Best estimate of r_c from above plots is $r_c = 0.001\,54$. By (4×4) Padé approximants, $r_c = 0.001\,538$.

and the bandwidth is obtained as $0.57 < \alpha R^{-\frac{1}{3}} < 0.64$ for the axisymmetric case and $0.15 < \alpha R^{-\frac{1}{3}} < 0.21$ for the non-axisymmetric case.

The fact that within the preferred band of α all the K_{ni} have the same negative sign (depicting tendency of amplification by the higher-order terms) enables us to draw at least one significant conclusion. That is, in this region there *has to be* a zero-crossing within the nearest singularity, if the nearest singularity is a simple pole. Thus the results qualitatively ensure the possibility of destabilization of the flow due to finite-amplitude effects.

We again take a look at tables 1 and 2, where K_{ni} coefficients are also given for values of $\alpha R^{-\frac{1}{3}}$ lying just outside the extremities of the preferred band. It appears from these coefficients that there could be a variety of reasons for the destruction of the feature of uniform negative sign of the K_{ni} coefficients. For instance, if the coefficients tend to change sign at higher orders it is possible that a weak secondary pole has moved inside the circle of convergence and thus become the primary singularity. Or, if periodic sign changes take place, then it is possible that a complex-conjugate secondary singularity has moved inside the circle of convergence and thus become the primary singularity. Or, it is also possible that a fresh but weak primary singularity has developed within the original circle of convergence. Whatever the nature or mechanism of the singularities, very detailed and critical analysis using both the Shanks (1955) method and Padé approximants (cf. Van Dyke 1974) showed that it is very difficult indeed to get any conclusive answers for the regions lying outside the preferred band. Thus, hereinafter, all the analysis presented, for both the axisymmetric and non-axisymmetric cases, will be restricted to the results within the preferred band only. Also, it is in view of this fact that the typical Domb–Sykes plots shown in figures 1 and 2 are for points well within the preferred band.

Later analysis will show that, whilst on the one hand the K_{ni} coefficients are of rather irregular magnitude, on the other hand (upon introducing scales given by Davey & Nguyen 1971) the K_{ni} coefficients, at different sets of values of α and R, depict near-perfect scaling when the value of $\alpha R^{-\frac{1}{3}}$ is the same. On this latter count, the analysis of results is to a large extent simplified.

4.2. *Determination of equilibrium amplitudes*

For reasons already mentioned, the attempts to determine the equilibrium amplitude were reasonably successful only for points within the preferred band wherein all the K_{ni} are of the same negative sign. After inspection of the magnitudes of the K_{ni} coefficients and of those of the (fictitious) equilibrium amplitudes A_n based on the direct sum of the series up to K_{ni} terms, it was concluded that the true equilibrium amplitude A_e would lie very close to the radius of convergence. Thus, with a very poor rate of convergence of the series (7), for levels of amplitude of the same order as A_e, it would be virtually impossible to obtain the true equilibrium amplitude A_e without recourse to some procedure of accelerated convergence. However, one feature was guaranteed at the outset; that is, within the preferred band, A_e would *have* to lie within the radius of convergence r_c, i.e. $A_e < r_c$, since all the K_{ni} are of the same negative sign. Regarding the use of accelerated convergence techniques, two methods were tried, namely the Shanks (1955) method and the method of Padé approximants (cf. Van Dyke 1974). Results based on both are discussed next.

For the axisymmetric case the Shanks method using the e_1^m transform did not yield sensible answers even with nine K_{ni} coefficients. This is because the higher order e_1^m transform columns showed no trend towards convergence for levels of $|A|$ of the same

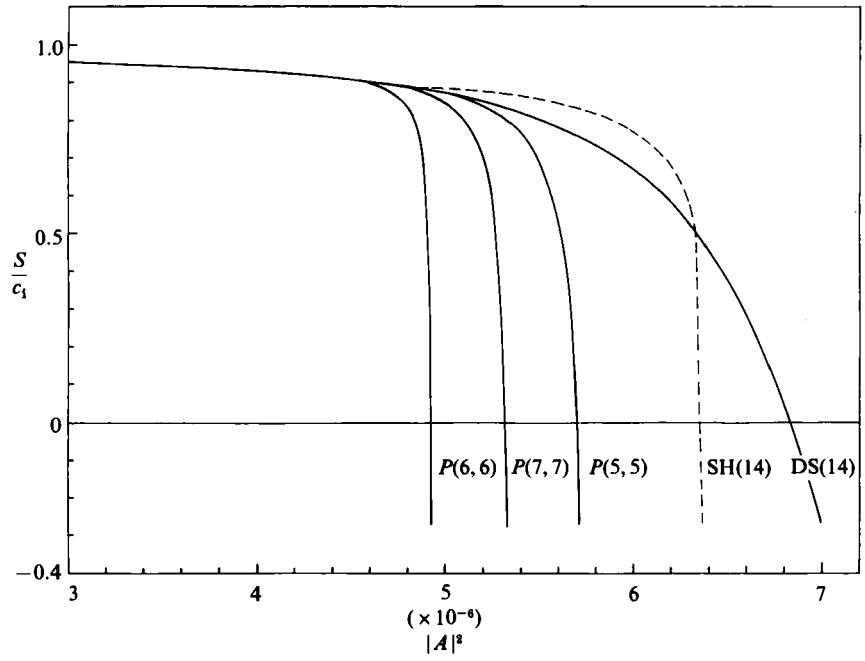

FIGURE 3. S/c_i versus $|A|^2$ for $\alpha = 11.0$, $R = 6000$, axisymmetric case. $P(m, m)$ represents curve based on $(m \times m)$ Padé approximants. SH(14) represents curve based on Shanks method and DS(14) represents curve based on direct sum of series, both using the first fourteen K_{ni} coefficients.

order as r_c. Using fourteen coefficients, convergence of e_1^m transform columns was obtained and a prediction of the zero-crossing of the series (7) could be made. However, more critical inspection showed that the result for A_e thus obtained was not entirely trustworthy. To understand this, we look at figure 3, where the normalized series (7) sum S/c_i is plotted versus $|A|^2$. It is seen in this figure that the sum according to the Shanks method is *greater* than the direct sum of the series up to fourteen K_{ni} coefficients, in a region where $|A|$ is less than the value predicted as the zero-crossing by the Shanks method. Now, if the sum according to the Shanks method is the 'true sum', then obviously in a region where $|A| < r_c$ this 'true sum' must be less than the direct sum up to a finite number of terms, because all the K_{ni} are of the same negative sign. Since the Shanks method gave the opposite result, it was concluded that the Shanks method was converging to the wrong answer. Shanks (1955) pointed out that this situation could arise if there is a double pole or two simple poles close to each other located on the real axis. We believe that the existence of a pair of complex-conjugate secondary singularities, lying outside the circle of convergence but with the real ordinate having a value less than r_c, is really the cause of the breakdown of the Shanks method, because the pair would simulate two singularities close to the real axis. Nevertheless, since it was found that the results obtained by the Shanks method are inconsistent and contradictory, the method was ultimately abandoned as being unsuitable for the problem in question. The e_2^m transform was also tried, but that too did not yield satisfactory results.

Next, for the axisymmetric case, Padé approximants were tried. Normalized sums for S/c_i, calculated on the basis of Padé approximants, are plotted versus $|A|^2$ in figure 3. The curves $P(5, 5)$, $P(6, 6)$ and $P(7, 7)$, respectively based on (5×5), (6×6)

and (7×7) Padé approximants, indicate a 15% scatter in the respective predicted values of A_e and r_c. This obviously calls for caution in the interpretation of results, especially considering Van Dyke's (1974) warning that one must look for a good deal of internal consistency before accepting results based on Padé approximants or the Shanks method. We thus look for consistency, if any, in the results. Our starting point is the series (7) itself, wherein we remember that all the K_{ni} coefficients are of the same negative sign and the nearest singularity is a simple pole. As stated earlier, this guarantees a zero-crossing of the series (7) within the nearest singularity, so that $A_e < r_c$. The results by Padé approximants, at all orders, confirm this and show that the numerator and denominator zero-crossings of the approximants occur very close to each other, with the former occurring for a value of $|A|^2$ slightly smaller than that for the latter. Incidentally, this feature is responsible for the sharp fall in the curves in figure 3. Moreover, the true series sum, as predicted by the approximants, is everywhere less than the direct sum up to a finite number (fourteen) of terms, and this result is consistent with the same negative sign of K_{ni}. Also, the r_c predicted by (7×7) Padé approximants is in very good agreement with the r_c predicted by Domb–Sykes plots as indicated in figure 1. Further, in figure 3 the $P(7, 7)$ curve is bracketed between the $P(5, 5)$ and $P(6, 6)$ curves. Whereas the above arguments are indicative of a good measure of consistency in the results, these do not explain the scatter in the results obtained. To understand this scatter, we turn to the Domb–Sykes plots in figure 1, which show that there is a very large variation in the magnitudes of K_{ni}, with a periodicity of four. It is therefore reasonable to expect that in these circumstances some scatter will be obtained in the predicted values A_e and r_c at different orders of Padé approximants. Thus, after considering all points, the best estimate of the true value of A_e that was used in the subsequent analysis was the one based on (7×7) Padé approximants. At the same time, owing to the scatter in the results for A_e and r_c, the reader is advised to exercise caution on two counts before accepting the results. First, some small degree of reservation must be maintained regarding the convergence of the series (7), at levels of $|A|$ of the order of A_e, despite the earlier mentioned powerful argument that A_e must be less than r_c. Secondly, a greater degree of reservation must be maintained regarding the *numerical* value of A_e based on (7×7) Padé approximants, although this value has been stipulated as the best estimate of the true value of A_e in the problem.

We next turn our attention to the non-axisymmetric problem. For this problem the first eight K_{ni} coefficients are available. To calculate still-higher-order K_{ni} enormous volume of computation would have to be done for every subsequent coefficient calculated. This is because of the many nonlinear terms on the right-hand sides of (26)–(28). This effort was not felt to be worthwhile for the following reasons. First of all, figure 2 indicates that the Domb–Sykes plots amply reveal the trend of the series within the first eight K_{ni}. Secondly, results by (4×4) Padé approximants give the value of r_c in perfect agreement with that based on the Domb–Sykes plots. Thirdly, the Padé approximants results show that A_e is very close to r_c, but with $A_e < r_c$, as is shown in figure 4, which accounts for the sudden drop in the S/c_i versus $|A|^2$ curve. Fourthly, the 'true-sum' curve is lower than the 'direct-sum' curve, which is consistent with all negative K_{ni}. Thus it is believed that more or less all of the information that can be extracted from the series is revealed to a reasonable extent within the first eight K_{ni}. Incidentally, the Shanks method using the e_1^m transform was also tried for this case. It was seen that the penultimate e_1^m column developed into an alternating series, near the zero-crossing of the series. To that extent, the method depicts a trend towards convergence, and it is believed that if

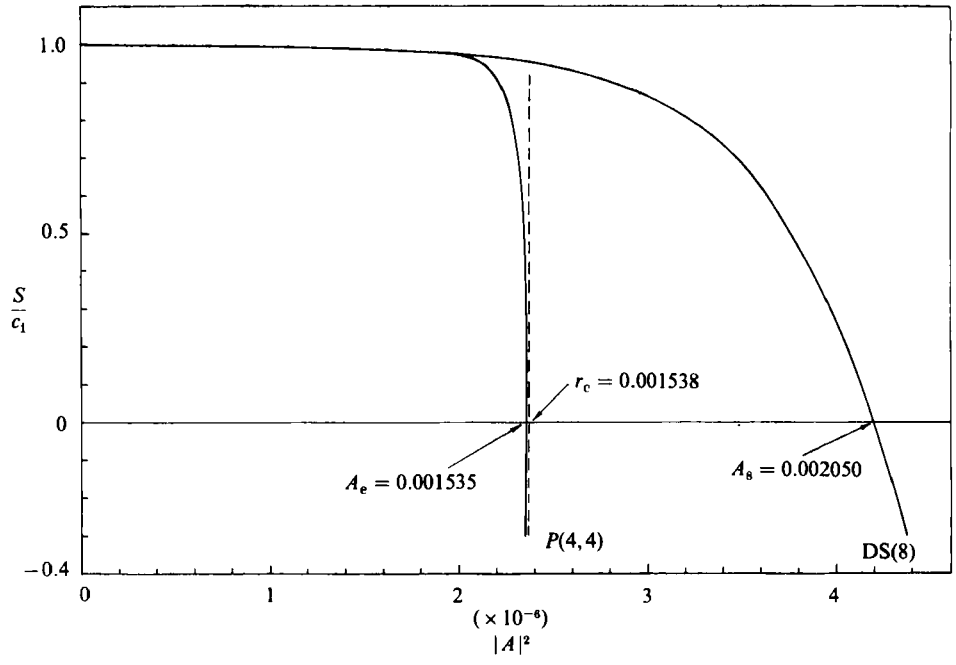

FIGURE 4. S/c_1 versus $|A|^2$ for $\alpha = 3.0$, $R = 5000$, non-axisymmetric case. $P(4,4)$ represents curve based on (4×4) Padé approximants. DS(8) represents curve based on direct sum of series using the first eight K_{n1} coefficients.

more terms were used an actually convergent answer would be obtained for the zero-crossing. Nevertheless, the value of A_e predicted by the Shanks method is in good agreement with that by (4×4) Padé approximants, within the preferred band, even with the first eight K_{n1}. Thus in the subsequent analysis of the non-axisymmetric problem the value of A_e used was based on (4×4) Padé approximants, and the degree of reservation on the accuracy of the numerical value of A_e is certainly less than that for the axisymmetric case. For the latter, the series is much more irregular even up to the first fourteen K_{n1}.

As a final observation in this subsection, it may be mentioned that no satisfactory or trustworthy values of A_e could be obtained for the regions lying outside the preferred band in either of the two cases.

4.3. *Consideration of scales*

The results obtained may be seen in fuller perspective upon considering the scales introduced by Davey & Nguyen (1971) and by Gill (in an appendix to Davey & Nguyen 1971). The most important result predicted by them was that R^2E is a function of $\alpha R^{-\frac{1}{3}}$. Also the minimum value of E, viz $E_{\min}$, is $E_{\min} \sim R^{-2}$, and $R^2E_{\min}$ is uniquely related to $\alpha R^{-\frac{1}{3}}$. The quantity E is the relative kinetic energy, and is defined as the ratio of the energy of the disturbances to that of the energy of the basic flow. The quantity was introduced by Davey & Nguyen (1971) and by Kuwabara (cited by Davey, private communication), and is given by

$$E = 12 \int_0^1 \tfrac{1}{2}(u'^2 + v'^2 + w'^2)\, r\, \mathrm{d}r, \tag{54}$$

where $w' = 0$ for the axisymmetric case. Now u', v' and w' can only be approximately evaluated as part of the present calculations. This is because the sums of various series like (8) and (24) would be needed to evaluate the velocities. And, with a poor convergence rate, the sums would be extremely sensitive to even slight errors in the value of A_e. Thus, at the expense of accuracy in favour of numerical stability, the velocities were approximately evaluated based on the fundamental only, and based on the calculated value of A_e. The respective expressions for the velocities are as follows:

axisymmetric

$$u' = \sqrt{2}\, A_e \frac{|\psi_1'|}{r}, \quad v' = \sqrt{2}\, A_e \alpha \frac{|\psi_1|}{r} \ldots; \tag{55}$$

non-axisymmetric

$$u' = \sqrt{2}\, A_e |f_1|, \quad v' = \sqrt{2}\, A_e |g_1|, \quad w' = \sqrt{2}\, A_e |h_1| \ldots. \tag{56}$$

Using (55) and (56), the working expressions for E are given for the axisymmetric and non-axisymmetric cases respectively as follows:

$$E = 12 A_e^2 \int_0^1 [|\psi_1'|^2 + \alpha^2 |\psi_1|^2] \frac{\mathrm{d}r}{r}, \tag{57}$$

$$E = 12 A_e^2 \int_0^1 [|f_1|^2 + |g_1|^2 + |h_1|^2] r \, \mathrm{d}r. \tag{58}$$

We will now arrive at certain asymptotic estimates of various quantities based on the scales given by Davey & Nguyen (1971). According to them, for the centre-mode in both the axisymmetric and non-axisymmetric cases, the scales for the radial distance r (up to the critical point) and the differential operator D ($\equiv \mathrm{d}/\mathrm{d}r$) are respectively given as $r \sim (\alpha R)^{-\frac{1}{4}}$ and $\mathrm{D} \sim (\alpha R)^{\frac{1}{4}}$. We next recall the normalization of the eigenfunctions in the two problems. For the axisymmetric case this is $\psi_1'' = 2$ at $r = 0$, and for the non-axisymmetric case it is $g_1 = 1$ at $r = 0$. Using the estimates of r and D and the normalizations adopted, scales may be deduced for any quantity in either of the two problems, for example $\psi_1' \sim (\alpha R)^{-\frac{1}{4}}$ and $f_1 \sim \alpha^{-\frac{3}{4}} R^{\frac{1}{4}}$. We will see subsequently that the use of these scales proves to be a powerful method of analysis.

To begin with we need to check whether or not R^2E actually is a function of $\alpha R^{-\frac{1}{3}}$. Using (57) and (58), plots of R^2E versus $\alpha R^{-\frac{1}{3}}$ are shown respectively for the axisymmetric and non-axisymmetric cases in figures 5 and 6. The results are convincing enough, and very satisfactorily bear out the contentions of Davey & Nguyen (1971). However, the R^2E curve for the non-axisymmetric case does not show a distinct minimum within the preferred band, and outside the preferred band results could not be predicted by the present calculations. Nevertheless, $\alpha R^{-\frac{1}{3}} = 0.2$ was taken as the tentative minimum point for the R^2E curve in the non-axisymmetric case. For the axisymmetric case a distinct minimum is indicated for the R^2E curve at $\alpha R^{-\frac{1}{3}} = 0.605$. This value is somewhat lower than that predicted by Davey & Nguyen (1971) based on $A_e = A_1$, i.e. based on the first Landau coefficient K_{11}. Moreover, the magnitudes of R^2E are seen to be very much lower than those predicted by Davey & Nguyen, for the obvious reason that their estimate of A_e, based on A_1, is very much larger than that based on the present calculations. To examine this feature we take a look at table 3, which compares results at $R = 500$ with $\alpha = 6.2$ and $\alpha = 4.84$. The former is approximately the point of minimum $A_e (= A_1)$ according to Davey & Nguyen. The latter is the point of minimum A_e based on (7×7) Padé

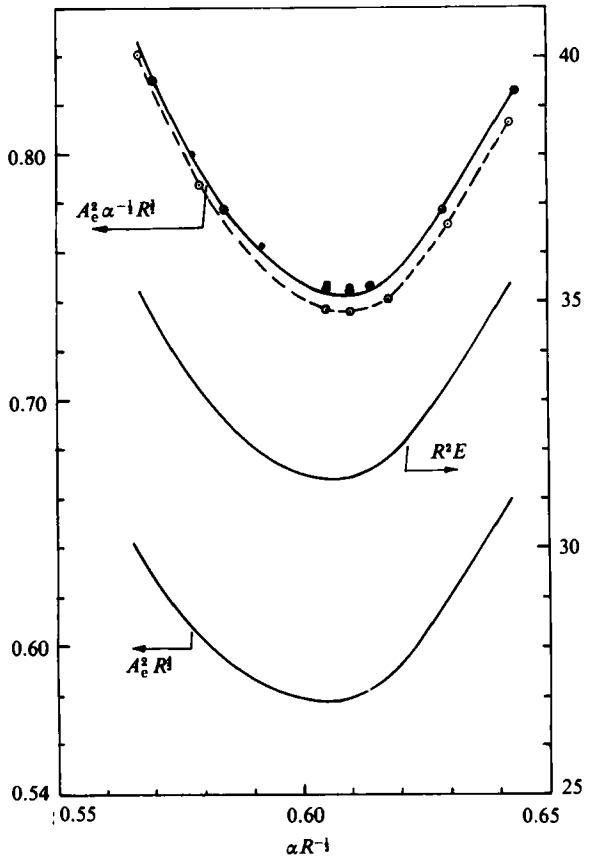

FIGURE 5. Different forms of fluctuation-energy levels plotted versus $\alpha R^{-\frac{1}{2}}$ for the axisymmetric case. Dispersion of results with R is illustrated in the $A_e^2\alpha^{-\frac{1}{2}}R^{\frac{1}{2}}$ curve. ——, $R = 4000$; – – · – –, 500; ⊗, 5000; ●, 6000.

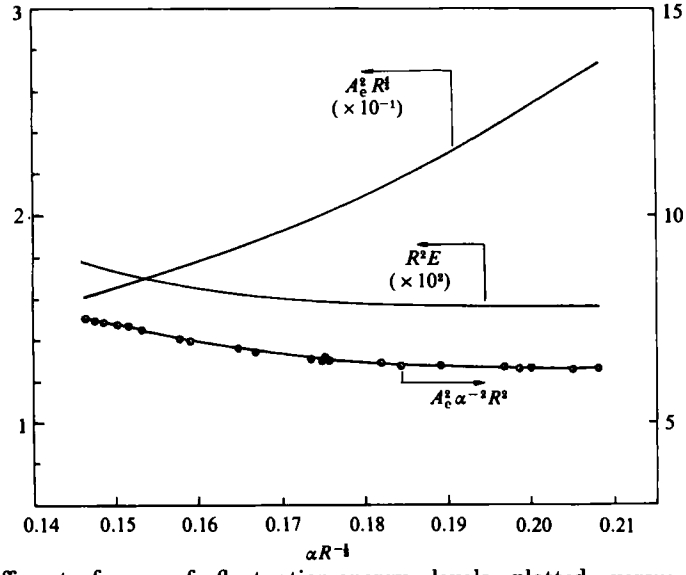

FIGURE 6. Different forms of fluctuation-energy levels plotted versus $\alpha R^{-\frac{1}{2}}$ for the non-axisymmetric case. Points shown on the $A_e^2\alpha^{-2}R^2$ curve are randomly chosen from the range $1000 \leqslant R \leqslant 5000$.

$\alpha = 6.2, R = 500, \alpha R^{-\frac{1}{3}} = 0.7812, c_r = 0.94920, c_i = -0.063200$, A_e not obtained by (7×7) Padé approximants				$\alpha = 4.84, R = 500, \alpha R^{-\frac{1}{3}} = 0.6048, c_r = 0.94250$, $c_i = -0.067176, A_e = 0.012036$		
n	K_{nr}	K_{ni}	A_n $(\times 10^{-2})$	K_{nr}	K_{ni}	A_n $(\times 10^{-2})$
1	2.3837	-2.3150×10	5.2250	3.2318	-2.2390×10	5.4763
2	1.5990×10^{4}	-1.3696×10^{5}	2.4495	-4.0471×10^{4}	-1.1426×10^{5}	2.5980
3	4.6515×10^{8}	-3.7336×10^{8}	2.0613	-2.4954×10^{8}	-2.0504×10^{8}	2.2496
4	5.6286×10^{12}	2.7621×10^{11}	—	4.8278×10^{11}	-5.6822×10^{11}	2.0776
5	2.4771×10^{16}	2.1843×10^{16}	—	5.6118×10^{15}	-1.1536×10^{16}	1.7784
6	-3.8356×10^{19}	2.6899×10^{20}	—	-3.8113×10^{18}	-8.2992×10^{19}	1.6355
7	-1.5169×10^{24}	1.8930×10^{24}	—	2.1512×10^{22}	-2.3694×10^{23}	1.5885
8	-1.7907×10^{28}	5.8328×10^{27}	—	1.9095×10^{27}	-1.2711×10^{27}	1.5505
9	-1.4793×10^{32}	-5.8737×10^{31}	1.7068	1.1098×10^{31}	-1.9497×10^{31}	1.4857
10	-5.8347×10^{35}	-1.2730×10^{36}	1.3779	2.4116×10^{34}	-1.3528×10^{35}	1.4427
11	4.4200×10^{39}	-1.3157×10^{40}	1.3013	4.3922×10^{38}	-5.3047×10^{38}	1.4223
12	1.0932×10^{44}	-7.9195×10^{43}	1.2703	5.8932×10^{42}	-4.1812×10^{42}	1.4010
13	1.1773×10^{48}	3.7272×10^{45}	—	3.2198×10^{46}	-4.3839×10^{46}	1.3753
14	7.5251×10^{51}	7.0235×10^{51}	—	1.4778×10^{50}	-2.4928×10^{50}	1.3586

TABLE 3. Results for $R = 500$ at $\alpha = 6.2$ and $\alpha = 4.84$ for the axisymmetric case. According to Davey & Nguyen (1971), the point of minimum equilibrium amplitude, based on K_1, is close to $\alpha = 6.2$ for $R = 500$, with $A_e = A_1 = 0.05225$. According to the present results, the point of minimum equilibrium amplitude, based on (7×7) Padé appriximants, is close to $\alpha = 4.84$ for $R = 500$, with $A_e = 0.012036$. A_n is the equilibrium amplitude based on direct sum of series up to the K_{ni}th term.

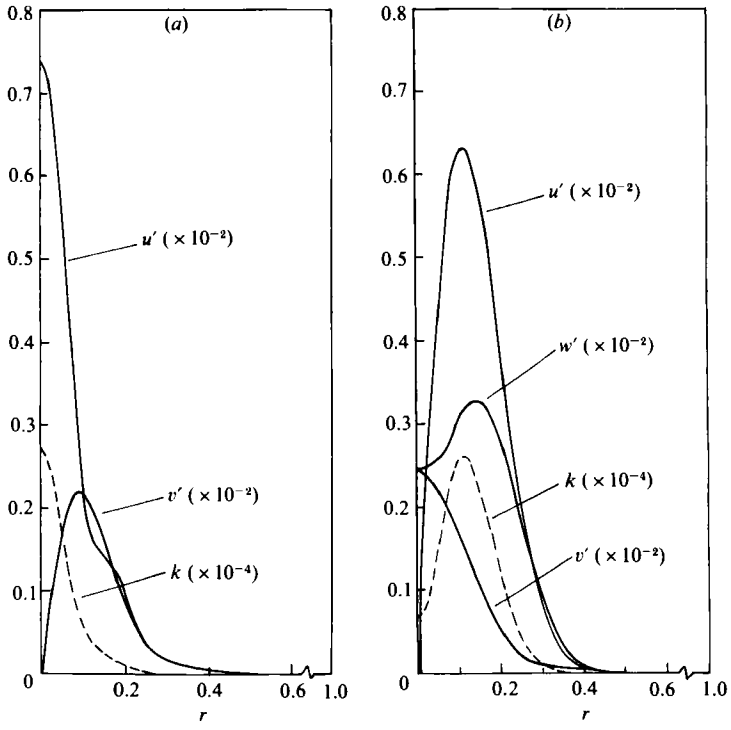

FIGURE 7. Distributions of the root-mean-squared velocities and the disturbance kinetic energy k. (*a*) Axisymmetric case with $\alpha = 10.341$, $R = 5000$, $\alpha R^{-\frac{1}{3}} = 0.605$. (*b*) Non-axisymmetric case with $\alpha = 3.42$, $R = 5000$, $\alpha R^{-\frac{1}{3}} = 0.200$. Both (*a*) and (*b*) correspond respectively to the minimum R^2E points obtained in each case.

approximants. We note further that $\alpha R^{-\frac{1}{3}} = 0.7812$ for $\alpha = 6.2$, which is well outside the preferred band. Further, (7 × 7) Padé approximants yield no result for A_e for this case. The comparative figures for A_e are as follows. For $\alpha = 6.2$, $A_e = A_1 = 0.05225$, whereas for $\alpha = 4.84$, $A_e = 0.01204$ by (7 × 7) Padé approximants. This accounts for the large difference in the R^2E values between the results of Davey & Nguyen and the present results. The comparison also illustrates that it is not safe to arrive at a result for A_e based on the first Landau coefficient alone.

Returning to the question of scales, it can easily be shown that the most prominent contribution to E is made by the u'^2 term in (54), both in the axisymmetric and non-axisymmetric cases. Consequently $R^2E \sim A_e^2 \alpha^{-\frac{1}{2}} R^{\frac{3}{2}}$ and $R^2E \sim A_e^2 \alpha^{-2} R^2$ in the axisymmetric and non-axisymmetric cases respectively. Figures 5 and 6 show that these two estimates are also functions of $\alpha R^{-\frac{1}{3}}$, and the respective curves have the same shape as the respective R^2E curves. These curves have also been used to illustrate the dispersion of data with differences in R, and it suffices to state that the larger the value of R the truer are the asymptotic estimates.

Now, once it is seen that $A_e^2 \alpha^{-\frac{1}{2}} R^{\frac{3}{2}}$ and $A_e^2 \alpha^{-2} R^2$ are functions of $\alpha R^{-\frac{1}{3}}$ in the two respective cases, it is obvious that the same quantities, multiplied by any multiple or power of $\alpha R^{-\frac{1}{3}}$, will also be functions of $\alpha R^{-\frac{1}{3}}$. On this basis it is easy to prove that $A_e^2 R^{\frac{4}{3}}$, $u'^2 R^{\frac{4}{3}}$, $v'^2 R^{\frac{4}{3}}$, $w'^2 R^{\frac{4}{3}}$ and $kR^{\frac{4}{3}}$ will all be functions of $\alpha R^{-\frac{1}{3}}$, where k is the disturbance kinetic energy,

$$k = \tfrac{1}{2}(u'^2 + v'^2 + w'^2), \tag{59}$$

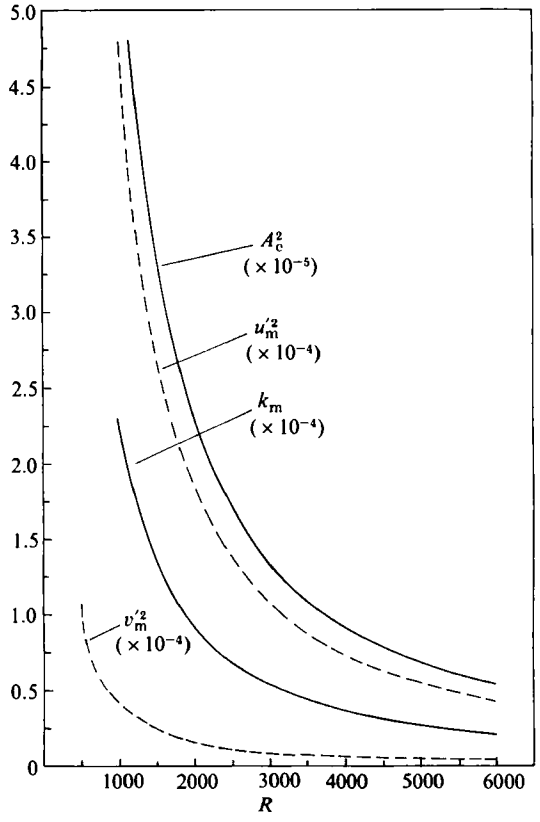

FIGURE 8. Variation of A_e^2, $u_m'^2$, $v_m'^2$ and k_m with R for the axisymmetric case at the minimum R^2E point, i.e. with fixed $\alpha R^{-\frac{1}{3}} = 0.605$. Subscript m refers to the maximum value in the range $0 \leqslant r \leqslant 1$. The asymptotic formulae are given as $A_e^2 R^{\frac{4}{3}} = 0.5789$, $u_m'^2 R^{\frac{4}{3}} = 4.631$. $v_m'^2 R^{\frac{4}{3}} = 0.4180$ and $k_m R^{\frac{4}{3}} = 2.3155$.

and $w' = 0$ for the axisymmetric case. Thus a plot of $A_e^2 R^{\frac{4}{3}}$ versus $\alpha R^{-\frac{1}{3}}$ is apparently the best way of depicting the equilibrium amplitude A_e, and these plots are also shown in figures 5 and 6.

We next take a look at plots of the disturbance velocity distributions shown in figure 7. These correspond to the minimum R^2E points in the axisymmetric and non-axisymmetric cases. The velocity fluctuations and k are calculated based on (55), (56) and (59). A remarkable result obtained is that the u'^2 fluctuation and k in the two cases are comparable, which would mean that both the axisymmetric and non-axisymmetric modes are equally likely to cause finite-amplitude destabilization.

Next at different values of R, but corresponding to $\alpha R^{-\frac{1}{3}} = 0.605$ for the axisymmetric case, and $\alpha R^{-\frac{1}{3}} = 0.200$ for the non-axisymmetric case (both being the respective minimum R^2E points), the different velocity fluctuations and k were calculated. Thereafter the respective maxima of these quantities in the range $0 \leqslant r \leqslant 1$ were found and plotted versus R. These quantities are indicated by the subscript m, and plots for them are shown in figures 8 and 9. The values of these quantities at $R = 4000$ provide the following set of asymptotic formulae:

axisymmetric

$$A_e^2 R^{\frac{4}{3}} = 0.5789, \quad u_m'^2 R^{\frac{4}{3}} = 4.631, \quad v_m'^2 R^{\frac{4}{3}} = 0.4180, \quad k_m R^{\frac{4}{3}} = 2.3155; \qquad (60)$$

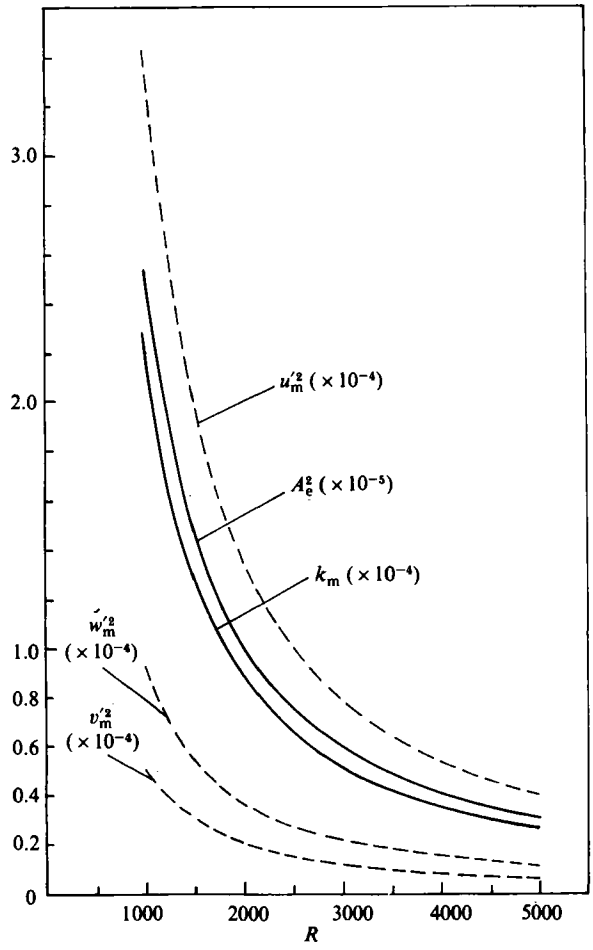

FIGURE 9. Variation of A_e^2, $u_m'^2$, $v_m'^2$, $w_m'^2$ and k_m with R for the non-axisymmetric case at the (tentative) minimum R^2E point, i.e. with fixed $\alpha R^{-\frac{1}{3}} = 0.200$. Subscript m refers to the maximum value in the range $0 \leqslant r \leqslant 1$. The asymptotic formulae are given as $A_e^2 R^{\frac{4}{3}} = 0.2536$, $u_m'^2 R^{\frac{4}{3}} = 3.401$, $v_m'^2 R^{\frac{4}{3}} = 0.5073$, $w_m'^2 R^{\frac{4}{3}} = 0.9214$ and $k_m R^{\frac{4}{3}} = 2.2213$.

non-axisymmetric

$$\left.\begin{aligned} A_e^2 R^{\frac{4}{3}} = 0.2536, \quad u_m'^2 R^{\frac{4}{3}} = 3.401, \quad v_m'^2 R^{\frac{4}{3}} = 0.5073, \\ w_m'^2 R^{\frac{4}{3}} = 0.9214, \quad k_m R^{\frac{4}{3}} = 2.2213. \end{aligned}\right\} \tag{61}$$

The above formulae and the curves shown in figures 8 and 9 provide a rational estimate of the size of disturbances at minimum threshold of destabilization. Incidentally, the plots in figures 8 and 9 are very close to what would be given by the asymptotic formulae respectively in (60) and (61). Also, as mentioned before, the formulae for k_m in (60) and (61) confirm that both are of virtually the same magnitude in the axisymmetric and non-axisymmetric cases.

The $R^2E_{\min}$ value has a different story to tell. For the axisymmetric case $R^2E_{\min} = 31$, and for the non-axisymmetric case $R^2E_{\min} = 155$. This is so because (54) can be rewritten as

$$E = 12 \int_0^1 kr \, dr, \tag{62}$$

	Axisymmetric case $\alpha = 4.80$, $R = 500$, $\alpha R^{-\frac{1}{3}} = 0.6048$, $c_r = 0.94226$, $c_i = -0.067335$, $A_e = 0.012021$, $c_i' = -0.067336$		Non-axisymmetric case $\alpha = 1.75$, $R = 1000$, $\alpha R^{-\frac{1}{3}} = 0.1750$, $c_r = 0.88486$, $c_i = -0.052265$, $A_e = 0.0044930$, $c_i' = -0.052344$	
n	K_{ni}	K'_{ni}	K_{ni}	K'_{ni}
1	-2.2296×10	-2.2293×10	-3.0063×10	-3.0092×10
2	-1.1274×10^{5}	-1.1190×10^{5}	-7.1931×10^{5}	-6.9135×10^{5}
3	-1.9148×10^{8}	-1.8275×10^{8}	-4.5301×10^{10}	-4.3800×10^{10}
4	-4.4560×10^{11}	-4.2703×10^{11}	-1.4423×10^{15}	-1.3780×10^{15}
5	-1.0634×10^{16}	-1.0600×10^{16}	-7.0981×10^{19}	-6.7855×10^{19}
6	-7.7986×10^{19}	-7.5769×10^{19}	-3.4127×10^{24}	-3.2636×10^{24}
7	-2.0685×10^{23}	-1.8662×10^{23}	-1.7010×10^{29}	-1.6293×10^{29}
8	-1.0181×10^{27}	-0.9618×10^{27}	-8.3879×10^{33}	-8.0515×10^{33}
9	-1.7533×10^{31}	-1.7194×10^{31}		
10	-1.2279×10^{35}	-1.1541×10^{35}		
11	-4.4661×10^{38}	-3.9070×10^{38}		
12	-3.5770×10^{42}	-3.3732×10^{42}		
13	-4.0146×10^{46}	-3.8198×10^{46}		
14	-2.2762×10^{50}	-2.0249×10^{50}		

TABLE 4. Illustration of the scaling of c_i and K_{ni} coefficients. c_i' and K'_{ni} are the scaled values of c_i and K_{ni} as obtained respectively from those at (i) $\alpha = 9.6$ and $R = 4000$ (given in table 1 for the axisymmetric case), and (ii) $\alpha = 3.0$ and $R = 5000$ (given in table 2 for the non-axisymmetric case). Values of $\alpha R^{-\frac{1}{3}}$, for the respective pair of points compared, are very nearly the same. The asymptotic estimates are $c_i \sim (\alpha R)^{-\frac{1}{2}}$ and $K_{ni} \sim (\alpha R)^{-\frac{1}{2}} (R^{\frac{4}{3}})^n$, and at the same value of $\alpha R^{-\frac{1}{3}}$ the proportionality constants are very nearly equal.

and, as may be seen from figures 7(a,b), the maxima of k occurs off the centreline for the non-axisymmetric case. Thus this is tantamount to a larger global volume of energy for the non-axisymmetric mode. On this last basis, it would appear that perhaps axisymmetric disturbances are more dangerous than non-axisymmetric ones, because, all other things being equal, the global volume of disturbance energy required for destabilization at minimum thresholds is five times less in the axisymmetric case than in the non-axisymmetric case. This result is just the opposite to what is predicted by the linear theory.

The last but not the least thing that we would like to discuss is the matter of the scales for c_i and K_{ni}. According to Salwen & Grosch (1972), an asymptotic estimate of $c(= c_r + ic_i)$ is

$$c = [1 - A_m(\alpha R)^{-\frac{1}{2}}] + i[B_m(\alpha R)^{-\frac{1}{2}}], \tag{62}$$

with A_m and B_m being different (approximate) constants in the axisymmetric and non-axisymmetric cases. We found that B_m was not quite a constant but actually almost an exact function of $\alpha R^{-\frac{1}{3}}$. Thus the estimate for c_i is $c_i \sim (\alpha R)^{-\frac{1}{2}}$, with the proportionality constant being the same at the same value of $\alpha R^{-\frac{1}{3}}$. Moreover, it can be shown that the asymptotic behaviour of K_{ni} should be like $K_{ni} \sim c_i (R^{\frac{4}{3}})^n$ or $K_{ni} \sim (\alpha R)^{-\frac{1}{2}} (R^{\frac{4}{3}})^n$, with the proportionality constant being the same at the same value of $\alpha R^{-\frac{1}{3}}$. This indeed proves to be a remarkable result, because it enables one to predict the values of K_{ni} from one value of R to another, at the same value of $\alpha R^{-\frac{1}{3}}$. Typical comparisons are shown in table 4, for both the axisymmetric and non-axisymmetric cases. The points considered in table 4 are within the preferred band, but we actually compared many points outside the preferred band as well, in both the cases. The results showed that not only were magnitudes comparable, but

also sign changes were faithfully reproduced at the same value of $\alpha R^{-\frac{1}{3}}$. This leads us to two more important conclusions. First, the preferred band itself scales with $\alpha R^{-\frac{1}{3}}$. Secondly, if detailed study of the problems is made at a particular value of R, and for various different values of α, then the results are more or less known at all other values of R, to a very fair degree of detail, based on similarity with respect to $\alpha R^{-\frac{1}{3}}$. In other words, the results are similar with respect to $\alpha R^{-\frac{1}{3}}$, and this is a feature that future workers employing other methods could capitalize upon. The results thus do credit to Davey & Nguyen's (1971) and Gill's estimate of scales.

As a final remark, we may mention that it would be worthwhile to have the present results checked by other methods, like Herbert's (1977) iterative method or Zhou's (1982) method. We do not anticipate that either of the exercises will be easy, because the ill-conditioning of the higher-harmonic equations will cause problems in either of these methods.

4.4. *Some discussion on earlier work*

It has been mentioned earlier that opposite signs for the first Landau coefficient were obtained respectively by Davey & Nguyen (1971) and by Itoh (1977*a*,*b*) for the centre-mode axisymmetric disturbances. Later Davey (1978) correctly, in our opinion, attributed this discrepancy to the fact that the Stuart–Landau series was being used close to the radius of convergence in both of the two formulations. This fact has actually been borne out by our results, as discussed earlier. With the series being used close to the radius of convergence, it would be misleading to draw conclusions regarding nonlinear stability based on the first Landau coefficient alone.

Otherwise, it also appears to us that the RP theory and Itoh's theory strictly speaking do not admit of a ready comparison, except in certain broad points as described by Davey (1978). Itoh's theory is non-monochromatic in the sense that free modes are allowed to exist not only for the fundamental but also for the mean motion and second harmonic. The RP theory, on the other hand, is monochromatic in the sense that, except for the fundamental, no free modes are allowed to exist for the harmonics or the mean motion, which are purely forced solutions. Secondly, Itoh's theory is valid within the ambit of the assumed order of magnitude scheme, viz $O(\epsilon)$ for the fundamental and $O(\epsilon^2)$ for the *free modes* of the mean motion and second harmonic. In fact his conclusions might have been different had he assumed the second-harmonic free mode to be $O(\epsilon)$, a possibility that he himself mentions (Itoh 1977*a*, p. 466).

Moreover, Itoh's theory is asymptotic in $\epsilon \to 0$, which means that the theory is meant to predict (within the ambit of the assumed order-of-magnitude scheme) whether the nonlinear terms are stabilizing or destabilizing for arbitrary though small values of ϵ in the limit $\epsilon \to 0$. Also, Itoh's theory is unable to describe the equilibrium state of the fundamental, whereas the RP theory, by its very nature, is valid only at the equilibrium state, i.e. for the particular value of $A = A_e$. Thus it is clear that the purposes and extent of the two theories are different, and strictly speaking each theory is valid within its own ambit of assumptions. Nevertheless, there is some merit in the broad comparisons made by Davey (1978) regarding the two theories, but we find it difficult to accept Itoh's (1977*b*, p. 479) statement that the RP method is "not applicable to the problem of pipe-Poiseuille flow". At least this contention is not borne out by our present advanced calculations based on the RP method.

We are grateful to Professor J. T. Stuart of Imperial College, London, for his suggestions and encouragement. Referees have give valuable advice which helped in revising an earlier draft.

REFERENCES

BATCHELOR, G. K. & GILL, A. E. 1962 Analysis of the stability of axisymmetric jets. *J. Fluid Mech.* **14**, 529–551.

DAVEY, A. 1978 On Itoh's finite amplitude stability for pipe flow. *J. Fluid Mech.* **86**, 695–703.

DAVEY, A. & DRAZIN, P. G. 1969 The stability of Poiseuille flow in a pipe. *J. Fluid Mech.* **36**, 209–218.

DAVEY, A. & NGUYEN, H. P. F. 1971 Finite-amplitude stability of pipe flow. *J. Fluid Mech.* **45**, 701–720.

FOX, J. A., LESSEN, M. & BHAT, W. V. 1968 Experimental investigation of the stability of Hagen–Poiseuille flow. *Phys. Fluids* **11**, 1–4.

GARG, V. K. & ROULEAU, W. T. 1972 Linear spatial stability of pipe–Poiseuille flow. *J. Fluid Mech.* **54**, 113–127.

HERBERT, T. 1977 Finite amplitude stability of plane parallel flows. In *Proc. AGARD Symp. on Laminar–Turbulent Transition*; *Paper* 3, AGARD-CP-224.

ITOH, N. 1977*a* Non-linear stability of parallel flows with subcritical Reynolds numbers. Part 1. An asymptotic theory valid for small amplitude disturbances. *J. Fluid Mech.* **82**, 455–467.

ITOH, N. 1977*b* Non-linear stability of parallel flows with subcritical Reynolds numbers. Part 2. Stability of pipe Poiseuille flow to finite axisymmetric disturbances. *J. Fluid Mech.* **82**, 469–479.

LEITE, R. J. 1959 An experimental investigation of the stability of Poiseuille flow. *J. Fluid Mech.* **5**, 81–96.

REYNOLDS, W. C. & POTTER, M. C. 1967 Finite-amplitude instability of parallel shear flows. *J. Fluid Mech.* **27**, 465–492.

SALWEN, H. & GROSCH, C. E. 1972 The stability of Poiseuille flow in a pipe of circular cross-section. *J. Fluid Mech.* **54**, 93–112.

SARPKAYA, T. 1975 A note on the stability of developing laminar pipe flow subjected to axisymmetric and non-axisymmetric disturbances. *J. Fluid Mech.* **68**, 345–351.

SEN, P. K. & VENKATESWARLU, D. 1983 On the stability of plane-Poiseuille flow to finite-amplitude disturbances, considering the higher-order Landau coefficients. *J. Fluid Mech.* **133**, pp. 179–206.

SHANKS, D. 1955 Non-linear transformations of divergent and slowly convergent sequences. *J. Maths & Phys.* **34**, 1–42.

STUART, J. T. 1960 On the non-linear mechanics of wave disturbances in stable and unstable parallel flows. Part 1. The basic behaviour in plane Poiseuille flow. *J. Fluid Mech.* **9**, 353–370.

THOMAS, L. H. 1953 The stability of plane Poiseuille flow. *Phys. Rev.* **91**, 780–784.

VAN DYKE, M. 1974 Analysis and improvement of perturbation series. *Q. J. Mech. Appl. Maths* **27**, 423–450.

WATSON, J. 1960 On the non-linear mechanics of wave disturbances in stable and unstable parallel flows. Part 2. The development of a solution for plane Poiseuille flow and for plane Couette flow. *J. Fluid Mech.* **9**, 371–389.

ZHOU, H. 1982 On the non-linear theory of stability of plane Poiseuille flow in the subcritical range. *Proc. R. Soc. Lond.* A **381**, 407–418.